JOURNAL OF GEOPHYSICAL RESEARCH, VOL. 102, NO. B5, PAGES 9887-9909, MAY 10, 1997

Scale lengths of shear velocity heterogeneity at the base of the mantle from *S* wave differential travel times

Thorne Lay and Edward J. Garnero

Institute of Tectonics and W. M. Keck Seismological Laboratory, University of California, Santa Cruz

Christopher J. Young

Geophysics Department, Sandia National Laboratory, Albuquerque, New Mexico

James B. Gaherty

Department of Earth, Atmospheric and Planetary Sciences, Massachusetts Institute of Technology, Cambridge

Abstract. Resolving the seismic velocity heterogeneity in the lowermost mantle is essential for understanding the chemical and dynamical processes operating in the boundary layer between the core and the mantle. Several regions of the lowermost mantle appear to have abrupt increases in shear velocity several hundred kilometers above the core-mantle boundary, at the top of the D" layer. This structure is revealed by seismic wave energy refracted by the velocity increase, resulting in an extra arrival (*Scd*) in teleseismic *S* wavetrains at distances from 65° to 95°. Anomalies in differential travel times of the extra arrival relative to direct *S* (which turns at shallower depths in the midmantle) or *ScS* (which reflects from the core-mantle boundary below the velocity increase) provide probes of the velocity heterogeneity in the lowermost mantle with better vertical resolution than provided by conventional *ScS-S* measurements. We explore the spatial patterns in *Scd-S*, *ScS-Scd*, and *ScS-S* differential time residuals for paths through the lower mantle beneath Alaska, Eurasia, and India (all being regions with coherent *Scd* phases) to place constraints on the strength and scale lengths of shear velocity heterogeneity and/or variable topography of the lower mantle discontinuity in these regions. The observed patterns are poorly predicted by existing global tomographic models. Significant small-scale heterogeneity, with lateral length scales of 200-500 km or less, exists even within regions that display a relatively uniform D" discontinuity structure over scale lengths of 1500-2000 km. The strongest travel time variations are associated with structure above the D" region, in contrast to common assumptions. Rapid lateral fluctuations in *ScS-Scd* differential times suggest that the anomalies accumulate within a relatively thin zone, less than the overall thickness of D". Correlations among the differential time anomalies indicate that *Scd* variations, ranging over about 4 s, are more pronounced than *ScS* variations and that the travel time fluctuations accumulate near the top of D" due to shear velocity heterogeneity of ±4% within a 50 km thick region and/or discontinuity topography of ±50 km, with scale lengths of 200-500 km. It appears that the upper portion of D" is much more heterogeneous than the deeper region. Heterogeneity within the layer appears to be decoupled from that at the top of the layer or in the overlying mantle.

Introduction

The core-mantle transition zone is believed to involve a complicated thermal and chemical boundary layer which influences the dynamics of both the mantle and core [e.g. *Stacey and Loper*, 1983; *Young and Lay*, 1987a; *Lay*, 1989, 1995; *Loper and Lay*, 1995]. After several decades of seismological analyses, there is general acceptance of the notion that the D" region, the lowermost few hundred kilometers of the mantle, has stronger velocity heterogeneity than is characteristic of the midmantle. However, current models of D" heterogeneity are very limited in resolution and global coverage. Large-scale (>2000 km) seismic tomography inversions for deep mantle *S* wave velocity structure are converging with respect to the gross spatial distribution of D" heterogeneity but still differ significantly in both the strength and radial extent of the velocity anomalies [e.g., *Masters et al.*, 1992; *Su et al.*, 1994; *Liu and Dziewonski*, 1994; *Li and Romanowicz*, 1996], and *P* wave velocity models are even less consistent. At shorter scale lengths, many localized studies of the shear velocity structure, primarily involving differential travel time anomalies between phases such as *S*, *ScS*, *SKS*, and *SKKS*, have provided information about the lateral and radial seismic velocity gradients, but the global coverage is quite sparse [e.g. *Lay*, 1983; *Lavely et al.*, 1986; *Woodward and Masters*, 1991; *Garnero and Helmberger*, 1993; *Grand*, 1994; *Wysession et al.*, 1994, 1995a,b; *Sylvander and Souriau*, 1996]. Seismic travel time analyses tend to provide limited radial

Paper number 97JB00331.
0148-0227/97/97JB-00331$09.00

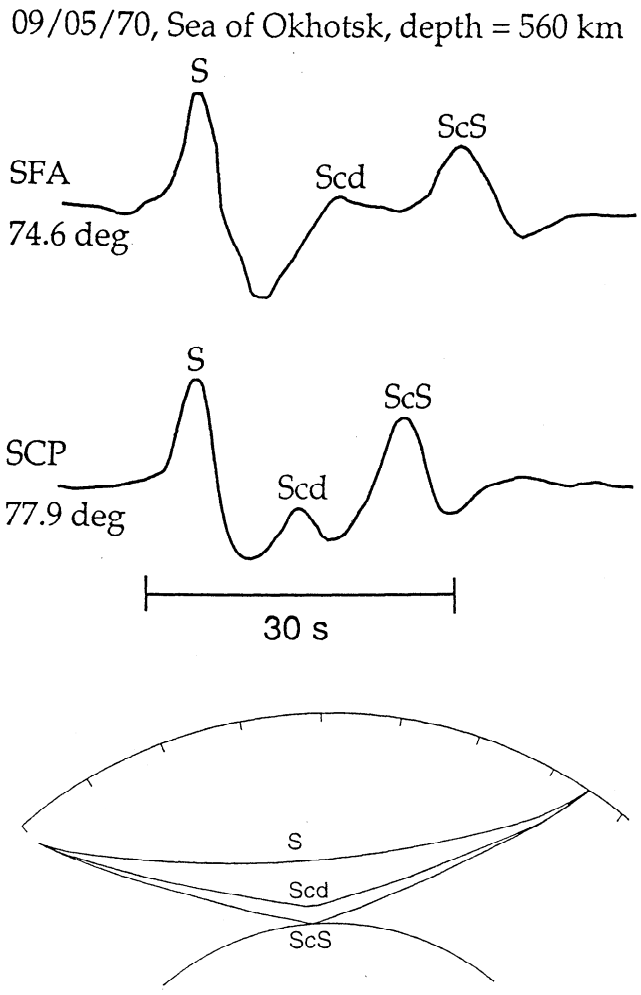

Figure 1. (top) Two examples of transverse component shear waves recorded by long-period seismometers for the deep earthquake of September 5, 1970. Standard Earth models predict the arrival of *S* and *ScS* but not the intermediate phase, labeled *Scd*. The latter phase can be modeled by introducing a 2.75% shear velocity discontinuity into the lower mantle, near 250 km above the core-mantle boundary. Refraction and reflection from this velocity increase produce a triplication of which the *Scd* arrival is the second forward branch. The timing of this phase relative to *S* and *ScS* is used in this paper to probe lowermost mantle heterogeneity. (bottom) Schematic ray paths for *S*, *Scd*, and *ScS* phases computed for model SYLO [*Young and Lay*, 1990] for a source at a depth of 500 km and a station at a distance of 75°. The *Scd* phase turns very close to the discontinuity in model SYLO (Figure 3), which is 243 km above the CMB.

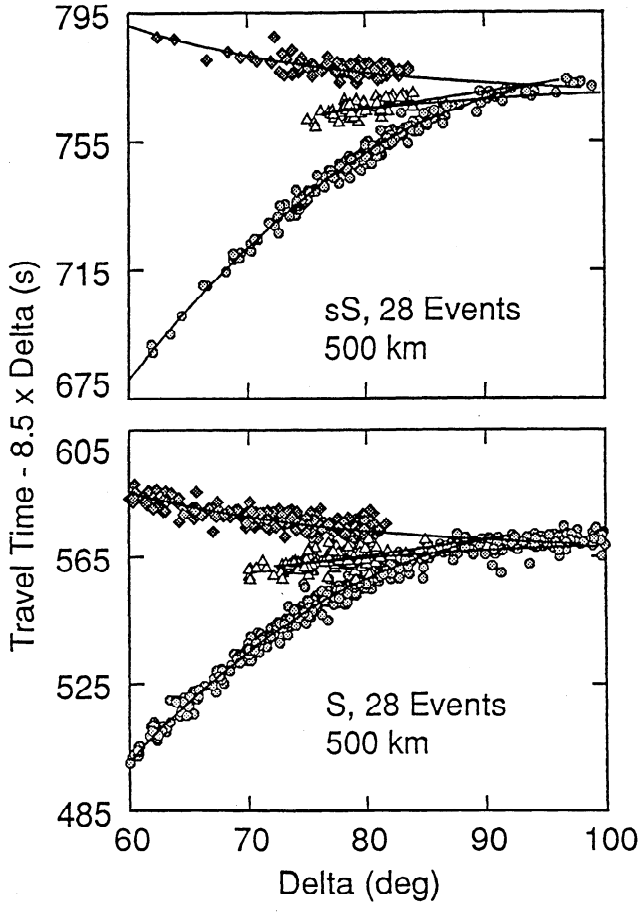

Figure 2. Travel time measurements from transverse component *S* wave recordings for 28 earthquakes in the western Pacific recorded at North American stations. The travel times have been adjusted to correspond to a source depth of 500 km. (top) Data from surface reflected phases. (bottom) Data for direct arrivals. Core reflections (*sScS* and *ScS*) are indicated by diamonds, first arrivals (*sS* and *S*) are indicated by circles, and the extra arrivals produced by a D" discontinuity (*sScd* and *Scd*) are indicated by triangles. The solid curves are computed for model SYLO (Figure 3), which has a 2.75% shear velocity discontinuity 243 km above the core-mantle boundary. *Young and Lay* [1990].

resolution of the velocity structure due to inadequate ray path coverage and the large differences in turning points of phases that are commonly used, such as *S*, *ScS*, and *SKS*.

The existence of reflecting boundaries within a medium enables superior vertical resolution of the structure to that achieved by turning wave travel time analysis. For example, *ScS-S* differential time anomalies, involving reflections from the core-mantle boundary (CMB), play a critical role in global tomography of the lower mantle. In some regions of the world, there is a rapid shear velocity increase within several hundred kilometers of the CMB which can provide an internal reference boundary for velocity structure analysis complementing the CMB itself. Reflections and refractions from this "shear velocity discontinuity" (the observations do not require that it be more abrupt than a 30 km wide transition zone) have been extensively observed in circum-Pacific regions that tend to have locally faster than average D" shear velocity in the large-scale global tomographic models [e.g., *Lay and Helmberger*, 1983; *Lay*, 1986; *Young and Lay*, 1990; *Weber and Davis*, 1990; *Revenaugh and Jordan*, 1991; *Gaherty and Lay*, 1992; *Garnero et al.*, 1993; *Weber*, 1993; *Kendall and Shearer*, 1994, 1995; *Kendall and Nangini*, 1996; *Ding and Helmberger*, 1996]. The seismic shear wave energy refracted by this discontinuity reaches the surface as an extra arrival between *S* and *ScS* in the distance range 65° to 85° (Figure 1), and strongly distorts the *S* waveforms from 85° to 95°. *Lay and Young* [1996] have demonstrated that the extra arrival originates near a surface at the top of D" rather than from isolated scattering structures. There are extra *P* wave arrivals from D" as well [e.g.,

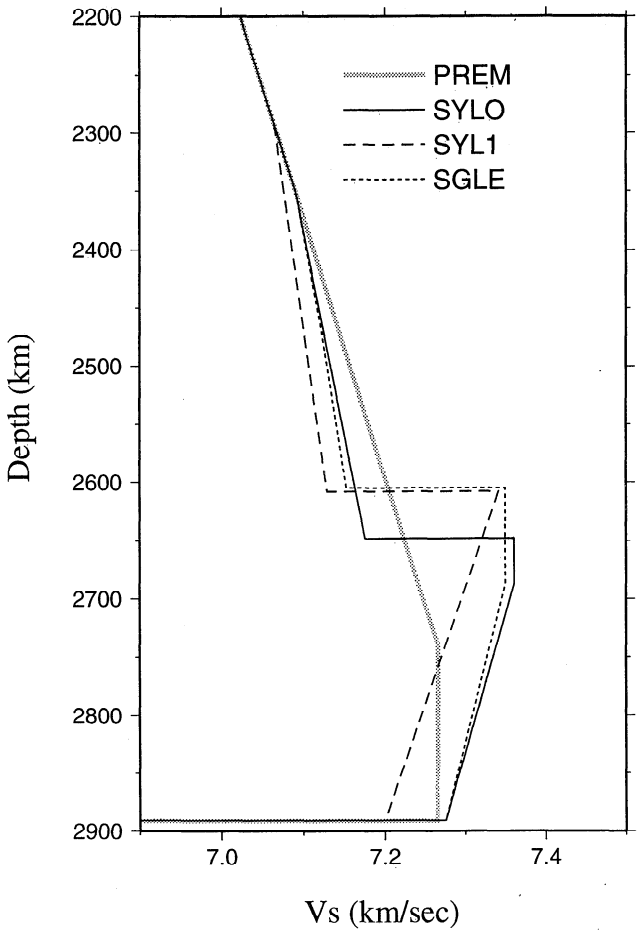

Figure 3. The three shear wave discontinuity models that serve as reference structures for the three regions considered in this paper, along with the 1 s shear velocity structure of model PREM [*Dziewonski and Anderson*, 1981]. Model SYLO [*Young and Lay*, 1990] is the reference model for paths under Alaska. Model SGLE [*Gaherty and Lay*, 1992] is the reference model for paths under Eurasia. Model SYL1 [*Young and Lay*, 1987b] is the reference model for paths under India.

Wright et al., 1985; *Weber and Davis*, 1990; *Houard and Nataf*, 1992, 1993; *Nataf and Houard*, 1993; *Weber*, 1993; *Vidale and Benz*, 1993; *Yamada and Nakanishi*, 1996], but the *P* velocity structure appears to be more variable [e.g., *Weber and Körnig*, 1992; *Weber*, 1993; *Krüger et al.*, 1993, 1995; *Ding and Helmberger*, 1996] and is less reliably used as a reference boundary.

In this paper, we exploit the existence of the extra *S* wave arrival, which we call *Scd* (following the nomenclature of *Lay and Helmberger* [1983]), and the associated D" shear velocity discontinuity to enhance our radial resolution of lowermost mantle heterogeneity in several regions. The extra arrival that we use for this purpose is actually a composite of energy turning just below the discontinuity (the true *Scd* phase) and energy reflected from the discontinuity (*Sbc*). In the long-period data that provide our differential times, only a single arrival can be measured because *Sbc* and *Scd* arrive very close together. The depth below the discontinuity at which *Scd* bottoms depends strongly on the velocity gradients in D", but simple models that predict the observed waveforms well indicate that the turning points are within a few tens of kilometers below the discontinuity for observations at distances of 70-83°, so the path difference between *Sbc* and *Scd* is very minor. Figure 1 illustrates the waveforms and ray path geometry characteristic of our data set, which involves long-period World-Wide Standardized Seismograph Network (WWSSN) recordings. To first-order, we can treat both *Scd* and *ScS* as reflections from boundaries with fairly well-constrained depths in the mantle, with differential times from which we derive the interval velocity corresponding to the integrated velocity anomaly through the D" region. Alternatively, one can infer boundary topography from the differential times, although this is more difficult to constrain because the presence of topography should produce larger ray path perturbations from the reference model than would volumetric heterogeneity. *Kendall and Shearer* [1994, 1995] mapped global lateral variations in the shear wave discontinuity depth using primarily *ScS-Sbc* observations and found large variations in apparent depth of the discontinuity. Comparison of *Scd-S* and *ScS-S* anomalies can be used to isolate the contributions of lower mantle heterogeneity above the D" discontinuity. We apply this approach to three regions of D" with lateral dimensions of 1500-2000 km that have stable *Scd* arrivals. Our focus is on mapping the variations down to scale lengths of 100-500 km, a significantly smaller scale that can presently be resolved using global travel time tomography.

Data

In this study, we utilize shear wave differential times obtained from three earlier investigations of separate regions of D". The most extensive data sets are for deep earthquakes in northwest Pacific subduction zones with paths traversing the D" region under Alaska [*Young and Lay*, 1990] and under northern Eurasia [*Gaherty and Lay*, 1992]. A smaller data set involves paths from Indonesian earthquakes sampling the deep mantle under India and the Indian Ocean [*Young and Lay*, 1987b]. Almost all tangential component shear waves traversing each of these regions are observed to have an extra arrival between direct *S* and *ScS* in the distance range 70° to 83°, indicating the presence of a shear velocity discontinuity about 250 km above the CMB in the sampled regions. Figure 1 shows representative examples of *S* waveforms recorded by long-period WWSSN and Canadian Seismic Network (CSN) seismometers, in this case for paths under Alaska. The ray paths shown in Figure 1 closely approximate the geometry for station SFA. The relative arrival time of the intermediate phase, *Scd* (+*Sbc*), can typically be measured with a precision of ±0.5 s for distances up to 80° and with somewhat higher uncertainty of ±1 s at larger ranges (due to interference with the instrument response from the first arrival, *S*). Typically, peak-to-peak differential time measurements prove most stable. We use the peak-to-peak differential time measurements from each of the three studies mentioned above, as we have found that more sophisticated waveform measurement procedures yield negligible differences [*Lay and Young*, 1996]. For each of the three regions, some of the data involve surface reflection phases, *sS*, *sScd*, and *sScS*, for which differential time measurements were computed in the same fashion as for direct arrivals. The measurements from the three studies were made in a self-

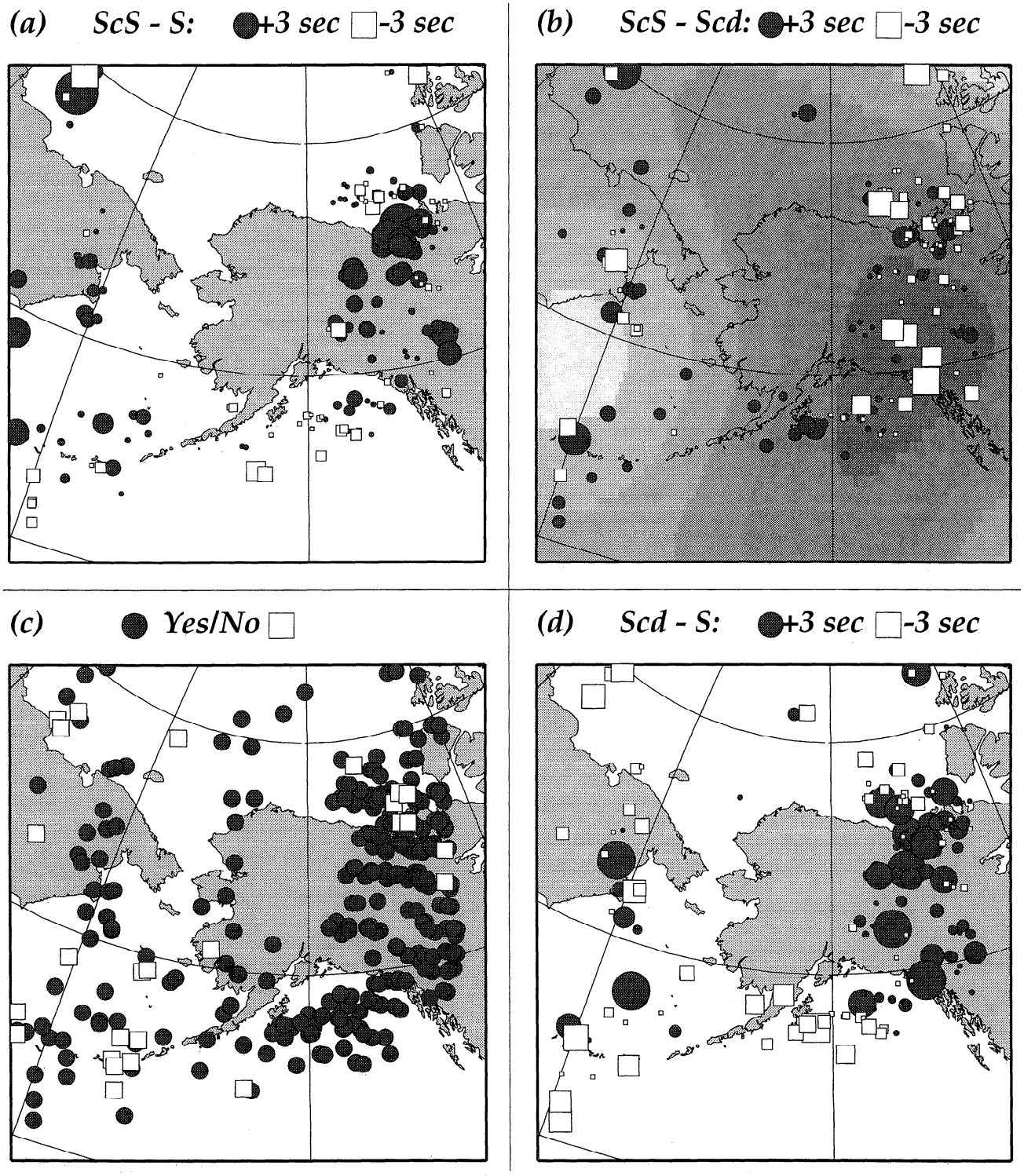

Figure 4. Differential travel time anomalies for (a) *ScS-S*, (b) *ScS-Scd*, and (d) *Scd-S* relative to model SYLO for paths under Alaska. Anomalies for surface-reflected phases are also included. The residuals are plotted at the *ScS* (or *sScS*) reflection point for each path. Anomalies with values of less than ±0.5 s are plotted with symbol sizes for values of ±0.5 s so that they are visible. (c) Map showing the midpoint of all paths in the data set of *Young and Lay* [1990], indicating whether an *Scd* phase was observed (yes) or not (no) for each case where model SYLO would predict an observable phase. In Figure 4b, the lateral shear velocity structure at a depth of 2800 km in the model *of Liu and Dziewonski* [1994] is indicated by shaded contours in 0.5% increments ranging from -0.5 to -1.0% slow (lightest shading) up to more than 1.5% fast (darkest shading) relative to PREM.

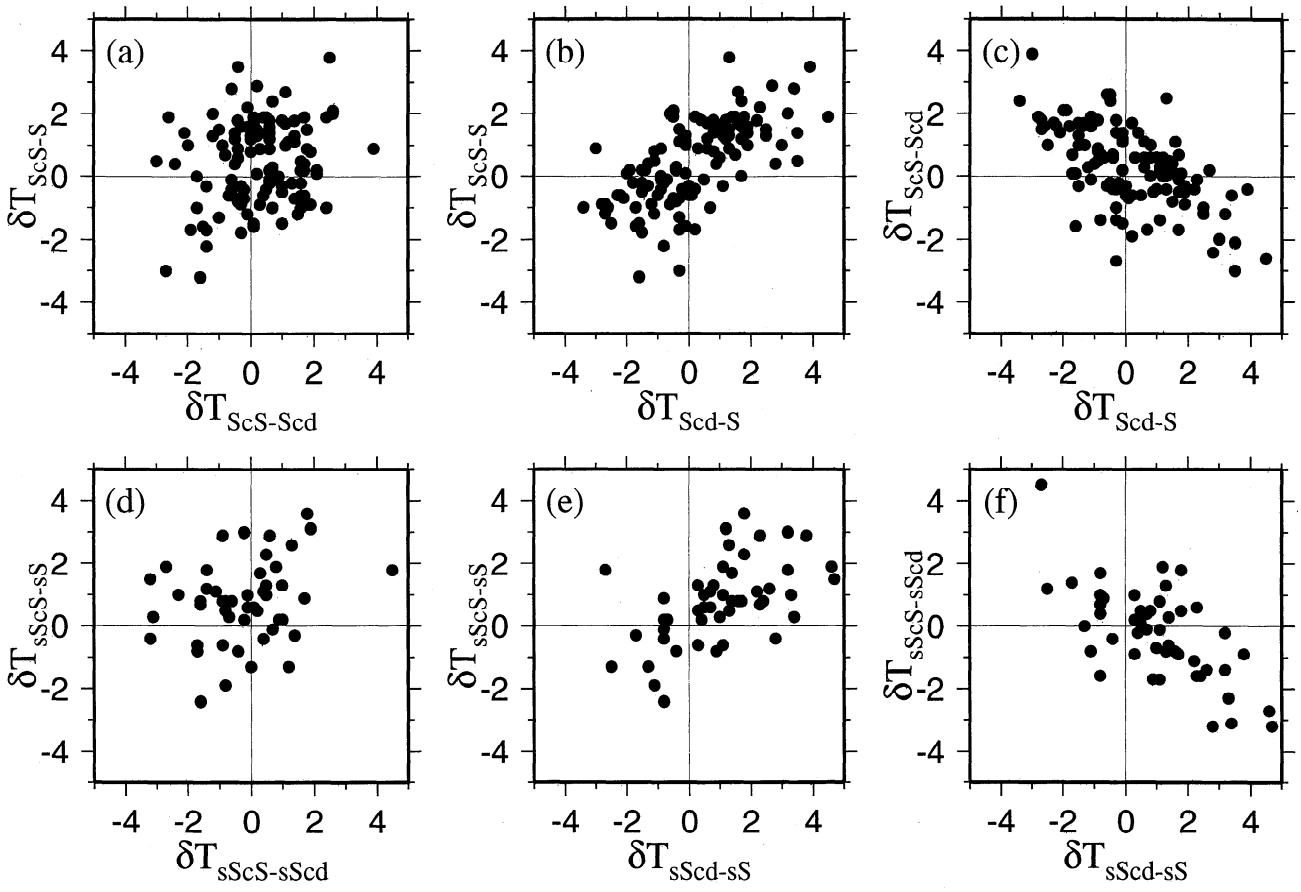

Figure 5. Scatterplots indicating the correlations between differential time anomalies for the (top) direct and (bottom) surface-reflected phases sampling the mantle under Alaska. (a) Differential anomalies with *ScS* in common. (b) Differential anomalies with *S* in common. (c) Differential anomalies with *Scd* in common. (d) Differential anomalies with *sScS* in common. (e) Differential anomalies with *sS* in common. (f) Differential anomalies with *sScd* in common.

consistent fashion, and while other data sets exist, they tend to provide only sparse coverage, lack the distance dependence that gives us confidence in the identification of the *Scd* arrival, and were measured using a variety of methods, so they are not included in this analysis.

Earlier work has established localized one-dimensional shear velocity models for each of our three regions that predict the first-order features of the long-period WWSSN travel times and waveforms, including the triplication effects giving rise to the *Scd* arrivals. An example of the fit provided by the best fitting one-dimensional model SYLO for the region under Alaska [*Young and Lay*, 1990] is shown in Figure 2. The data set sampling the mantle beneath Eurasia is fit comparably well by model SGLE [*Gaherty and Lay*, 1992] and for that below India by model SYL1 [*Young and Lay*, 1987b]. The three lower mantle structures vary slightly in the depth of the 2.75% shear velocity discontinuity in each region, and in the velocity gradients below the discontinuity (Figure 3). These localized models provide reference structures relative to which differential travel time anomalies are computed by differencing observed and predicted times for *Scd-S*, *ScS-Scd*, and *ScS-S*. Figure 2 indicates that differential time anomalies vary by about ±3 s for each of the phase pairs, which certainly exceeds the measurement accuracy. The use of localized reference models is necessary, given that standard Earth models such as PREM [*Dziewonski and Anderson*, 1981] lack the lower mantle shear velocity increase that gives rise to the *Scd* triplication phase.

While the differences in the background models for each region (inferred from baseline shifts in *ScS-Scd* differential times) are of great interest themselves, our primary focus is on the smaller-scale variations that exist within the 1500-2000 km wide patches sampled by the separate data sets. The three regions chosen for this analysis represent a relatively similar set of patches in that the basic discontinuity structure varies only slightly between regions (Figure 3). This is desirable in that we can assess the small-scale heterogeneity within relatively uniform large-scale provinces. Other areas show much more pronounced variations in the depth of the discontinuity of over 100 km [e.g., *Kendall and Shearer*, 1994] or lateral vanishing of the discontinuity over a limited region [e.g., *Garnero et al.*, 1988; *Weber*, 1993; *Kendall and Shearer*, 1995; *Kendall and Nangini*, 1996]. In such regions, the validity of using any one-dimensional reference model is questionable, and the very nature of the intermittent *Scd* phase is unclear. Rapid fluctuations in the *Scd* arrival may indicate scattering from a reflector with significant topography, or from discrete scattering structures [*Lay and Young*, 1996]. While restricting our attention to regions of greater waveform stability may tend to underestimate global D" heterogeneity, it does provide a sound basis for using differential time anomalies involving the *Scd*

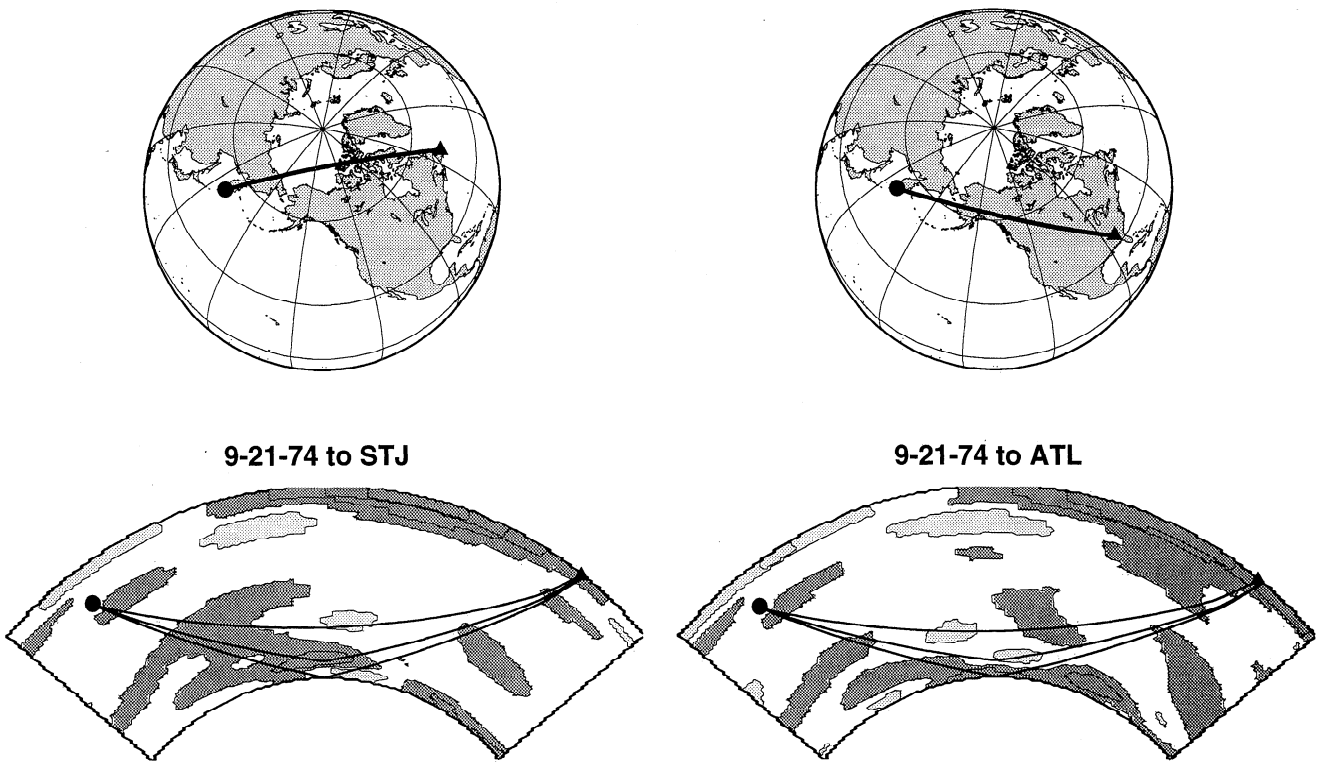

Figure 6. Great circle paths from a Sea of Okhotsk earthquake (September 21, 1974) to two stations in North America (STJ and ATL) along with cross sections through the aspherical shear velocity model of *Liu and Dziewonski* [1994]. The regions with dark shading are for regions with shear velocity that is more than 0.5% faster than average, while the light-shaded regions have shear velocity that is -0.5% or more slower than average. The contour intervals are at every 1% in velocity anomaly. Note the faster than average D" region in this model and the lateral variations affecting all phases.

phase in order to improve resolution of the lowermost mantle structure in regions with similar large-scale structure. Determination of the characteristics of D" structure on a local scale is just as important to resolving the processes in the boundary layer as is global imaging of the structure.

Differential Time Anomalies

For each of the three regions under consideration, we compute the differential time anomalies relative to the local reference model and then plot the anomalies on maps using the CMB reflection point of the *ScS* phase to each station. While this provides a useful display of spatial patterns in the data, it is important to keep Figure 1 in mind, as the associated raypaths for *S*, *Scd,* and *ScS* all have horizontally extended path lengths in the turning-point regions where the ray paths are sufficiently separated to allow differential travel time anomalies to accumulate. The frequency content of our signals should also be considered, as the predicted Fresnel zone for the grazing long-period S waves is more than 500 km [*Lay and Young*, 1996]. We will consider the finite path effects after assessing the point-wise properties.

The data set sampling the lower mantle below Alaska is displayed in Figure 4. In this case the ray paths traverse Figure 4 from left (sources in the northwest Pacific subduction zones) to right (stations in North America), and there is very little crossing ray coverage. In addition to showing the *ScS-S*, *ScS-Scd,* and *Scd-S* anomalies with respect to model SYLO, Figure 4c shows a bimodal waveform classification scheme from *Young and Lay* [1990], in which a yes symbol (solid circle) indicates that the corresponding observation did have an *Scd* arrival while a no symbol (open square) indicates that it did not. The yes/no plot suggests that a lower mantle discontinuity is coherent over a large-scale area in this case, with the region below the Aleutians having more mixed waveform behavior. *Young and Lay* [1990] consider the yes/no plot in further detail. The differential time anomalies shown are a subset of the total data set, involving only those seismograms with a clear *Scd* (or *sScd*) arrival in the distance range 70° to 83°. Points in the yes/no plot that lack differential travel time measurements in Figures 4a, 4b, and 4d correspond to observations from distances beyond 87°, where waveform distortions occur in the postcrossover region of the triplication. The geographical persistence of the *Scd* arrival should be kept in mind when evaluating differential times involving this phase. In regions where the phase is intermittent, it is more likely to be inappropriate to interpret it in the context of a one-dimensional reference structure.

Another feature of Figure 4 is that the shear velocity heterogeneity at a depth of 2800 km from the SKS12WM13 model of *Liu and Dziewonski* [1994] has been superimposed on Figure 4b. The darker areas are faster velocity, with a total range of velocity variation of 3% in this region. This model predicts relatively fast *ScS* times (yielding negative *ScS-S* and *ScS-Scd* differential time anomalies, if hetero-

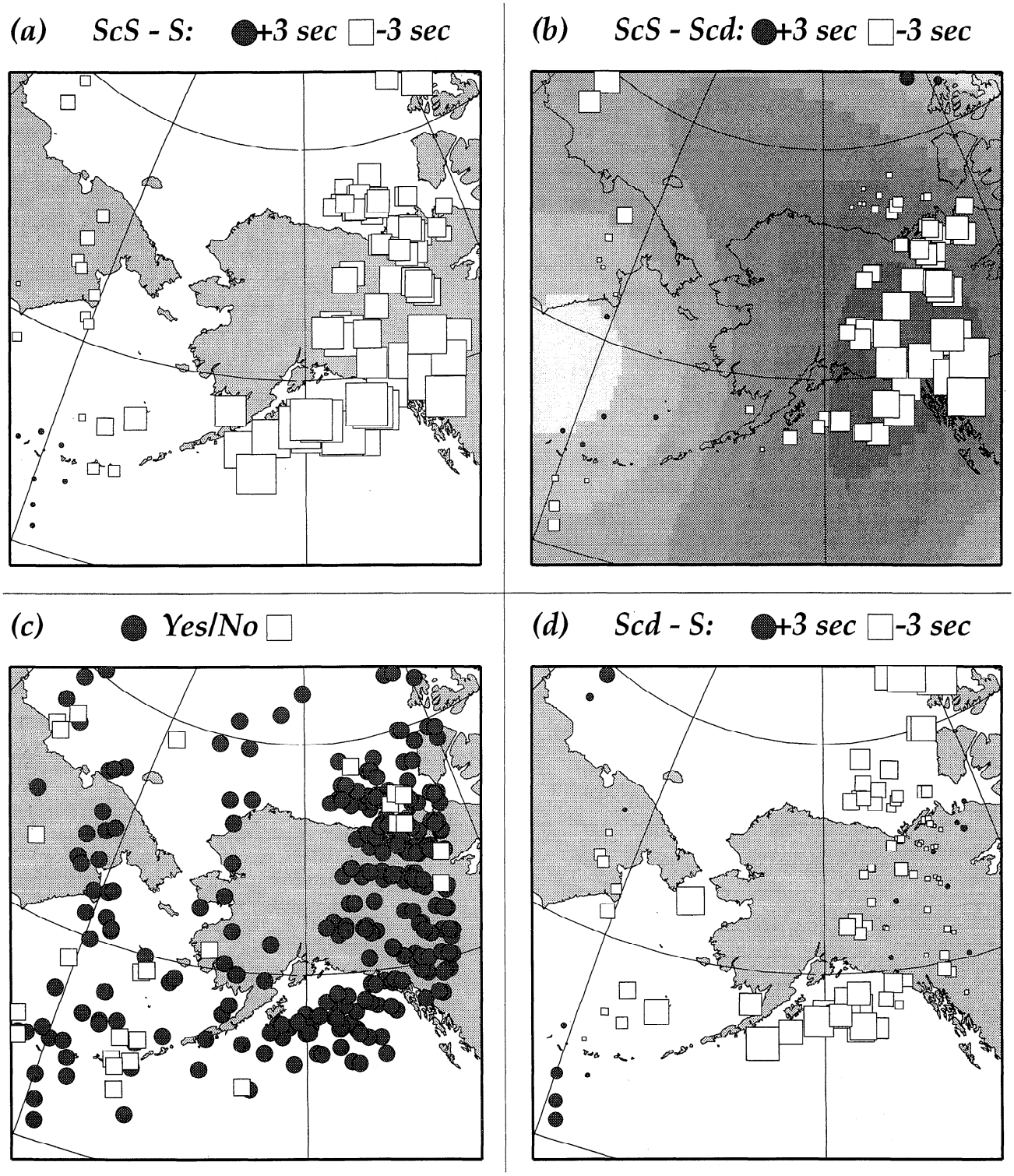

Figure 7. Predicted differential travel time anomalies for (a) *ScS-S*, (b) *ScS-Scd*, and (d) *Scd-S* using model SKS12WM13 [*Liu and Dziewonski*, 1994], adjusted to have model SYLO as a reference structure for paths under Alaska. Anomalies for surface-reflected phases are not computed. The residuals are plotted at the *ScS* reflection point for each path. Anomalies with values of less than ±0.5 s are plotted with symbol sizes for values of ±0.5 s so that they are visible. (c) Map showing the midpoint of all paths in the data set of *Young and Lay* [1990], indicating whether an *Scd* phase was observed (yes) or not (no) for each case where model SYLO would predict an observable phase. In Figure 7b, the lateral shear velocity structure at a depth of 2800 km in the model of *Liu and Dziewonski* [1994] is indicated by shaded contours in 0.5% increments ranging from -0.5 to -1.0% slow (lightest shading) up to more than 1.5% fast (darkest shading).

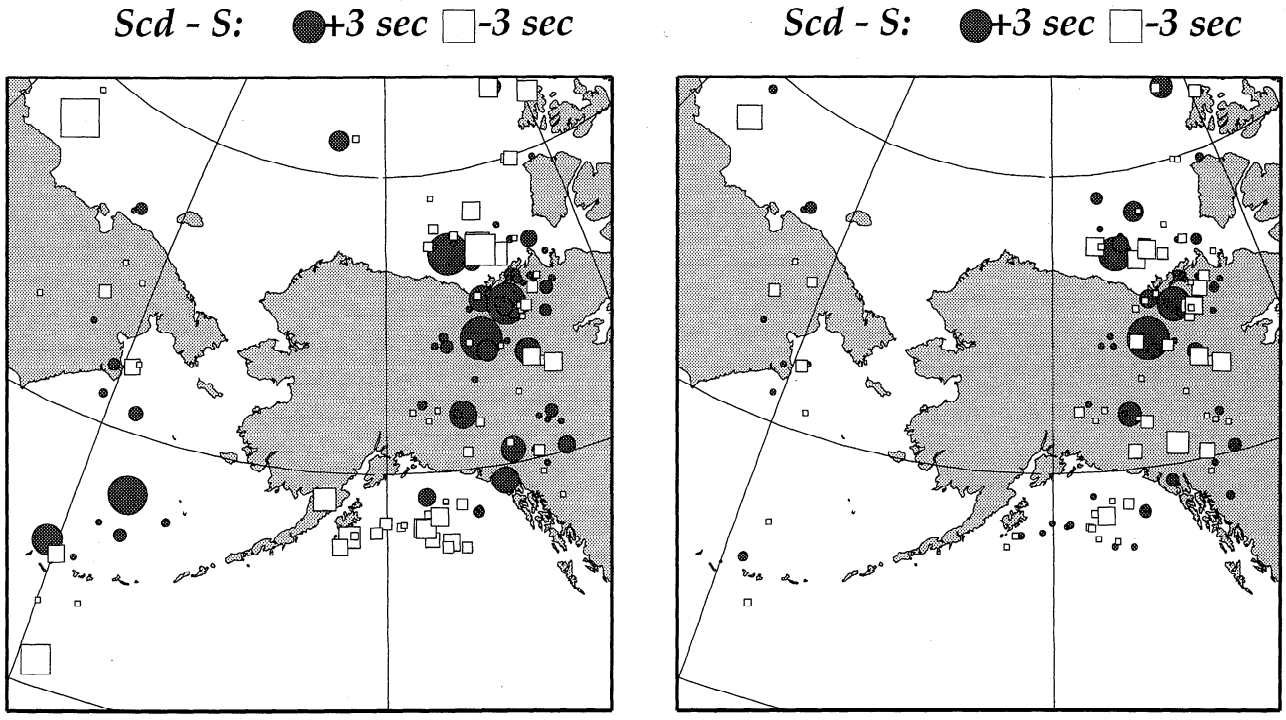

Figure 8. Differential travel time anomalies for *Scd-S* relative to model SYLO for paths under Alaska, corrected for (left) average source terms and (right) both source and station terms. Anomalies for surface-reflected phases are also included, with separate source terms, but common station terms. The residuals are plotted at the *ScS* (or *sScS*) reflection point for each path. Anomalies with values of less than ±0.5 s are plotted with symbol sizes for values of ±0.5 s so that they are visible.

geneities at shallower depths do not override the effect) for paths traversing the high-velocity region. In fact, some of the most negative *ScS-Scd* anomalies are centered in the high-velocity area, but this is not the case for *ScS-S* anomalies (Figure 4a), suggesting the presence of large travel time variations in direct *S*, at depths above the D" layer.

The overall patterns in Figure 4 are somewhat surprising, in that the amplitude of variations in *ScS-S* anomalies is comparable to that for *ScS-Scd* anomalies, while the pattern for *Scd-S* (involving phases that never traverse the D" layer at all) has the largest range and the most systematic large-scale coherence. From Figure 1, we might expect *ScS-S* anomalies to be the most variable, as the ray paths differ most for these phases, and the conventional "wisdom" has been that D" is more heterogeneous than the overlying mantle. Visually, the coherence of the *ScS-S* and *Scd-S* patterns is quite high, and there is a negative correlation between the *ScS-Scd* and *Scd-S* patterns. The paths traversing D" appear to sample somewhat smaller scale length structures, and there is no obvious relationship between *ScS-Scd* anomalies and the pattern of yes/no observations of the *Scd* phase.

These trends are quantified in Figure 5, which establishes the correlations between the differential time anomalies for direct phases and surface reflections separately. The linear correlation coefficients between the anomalies are 0.65 for *ScS-S* and *Scd-S*, 0.20 for *ScS-S* and *ScS-Scd*, and -0.61 for *ScS-Scd* and *Scd-S*. The surface reflections have similar coefficients of 0.54 for *sScS-sS* and *sScd-sS*; 0.27 for *sScS-sS* and *sScS-sScd*, and -0.67 for *sScS-sScd* and *sScd-sS*. The strong correlations when direct *S* is included in both terms indicate that indeed there are very large travel time variations, ranging over about 5 s, affecting the direct *S* waves and/or the *ScS* and *Scd* phases at depths above the D" region. The strong pattern in the direct *S* waves relative to *ScS* has been noted by *Lay* [1983] and *Schwartz et al.* [1991a]. In tomographic studies using *ScS-S* differential time anomalies there is a tendency to attribute most of the variance in the residuals to structure in D" (by the way the model is parameterized and sampled; usually sparse sampling of D" leads strong heterogeneity to be projected there), and this appears to be incorrect for this region. This is reinforced by the strong negative correlations for the pairs with *Scd* in common, given that *Scd* does not sample the D" region other than at the very top. It appears that much of the power in the *ScS-Scd* anomalies is associated with *Scd* fluctuations. In fact, the low correlations for the pairs where *ScS* is in common indicate that the pattern of heterogeneity within D" is decoupled from that in the overlying mantle (at least with respect to any topography in the D" discontinuity that gives rise to fluctuations in *Scd* arrival times).

We can use global tomographic models to try to reduce contributions from large-scale structure affecting the differential travel times. We consider the three-dimensional shear velocity model SKS12WM13 of *Liu and Dziewonski* [1994] for this purpose. Cross sections through that model for two paths traversing the mantle under Alaska are shown in Figure 6. Generally high velocities are found in D" for this area, but the direct S phases are not expected to encounter very extensive regions of fast material. While the model has lateral resolution only of the order of 2000-3000 km in the lower mantle, it is clear that differential times for the *S*, *Scd*, and *ScS* paths through this structure are expected to vary due to the separate paths through the mantle. Even though the level of velocity variation is small, the path lengths are

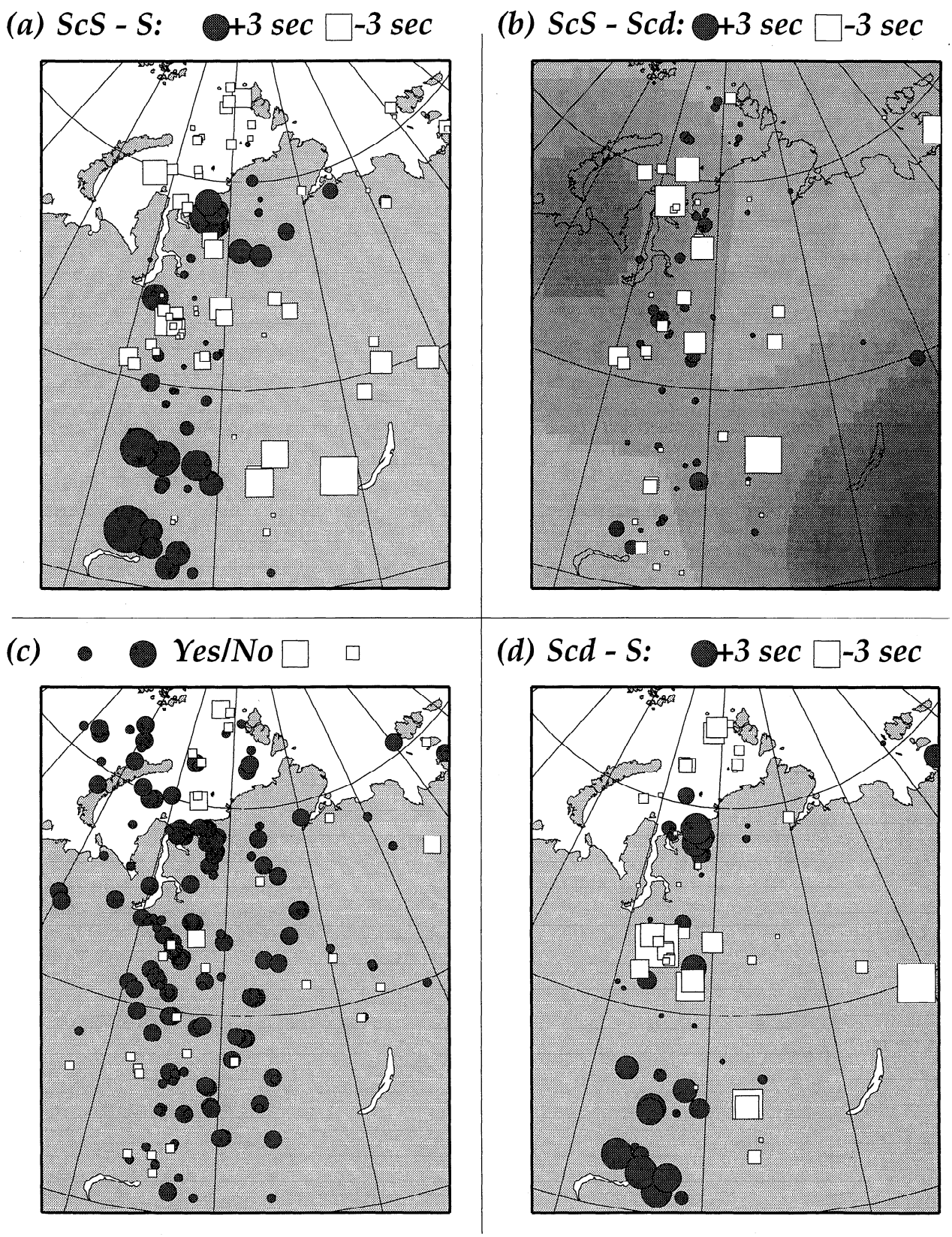

Figure 9. Differential travel time anomalies for (a) *ScS-S*, (b) *ScS-Scd*, and (d) *Scd-S* relative to model SGLE for paths under Eurasia. Anomalies for surface-reflected phases are included. The residuals are plotted at the *ScS* (or *sScS*) reflection point for each path. Anomalies with values of less than ±0.5 s are plotted with symbol sizes for values of ±0.5 s so that they are visible. (c) Map showing the midpoint of all paths in the data set of *Gaherty and Lay* [1992], indicating whether an *Scd* phase was observed (yes) or not (no) for each case where model SGLE would predict an observable phase. Two symbol sizes are used to indicate the confidence in the decision about whether *Scd* is present, with larger symbols reflecting higher confidence one way or another. In Figure 9b, the lateral shear velocity structure at a depth of 2800 km in the model of *Liu and Dziewonski* [1994] is indicated by shaded contours in 0.5% increments ranging from 0.0 to -0.5% slow (lightest shading) up to more than 2.0% fast (darkest shading).

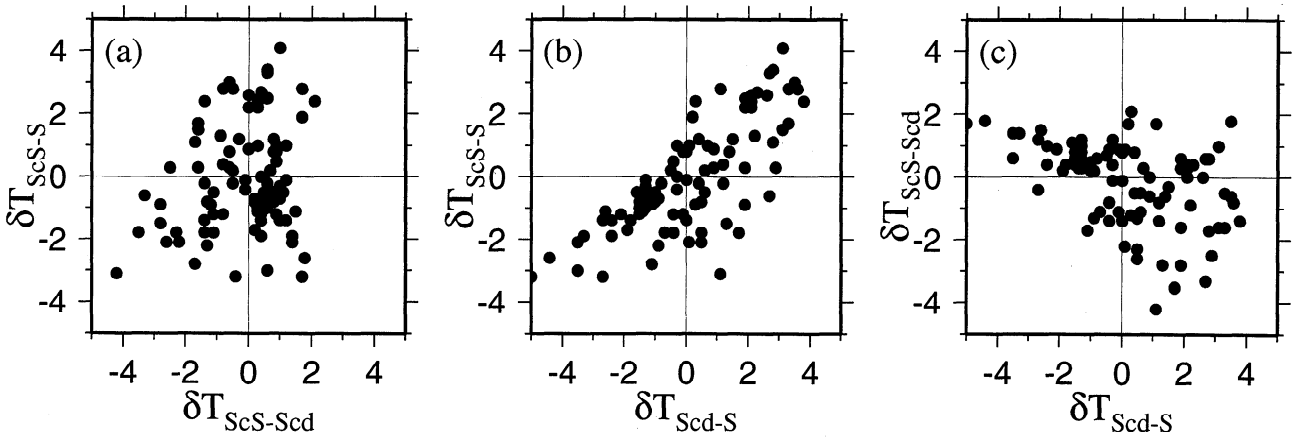

Figure 10. Scatterplots indicating the correlations between differential time anomalies for the direct phases sampling the mantle under Eurasia. (a) Differential anomalies with *ScS* in common. (b) Differential anomalies with *S* in common. (c) Differential anomalies with *Scd* in common.

long, allowing significant, several second, anomalies to accumulate along each ray path, giving rise to differential times on the same order as those in the data. Assuming homogeneous model ray paths (for model SYLO), the travel time anomalies through this structure were integrated along the *S*, *Scd*, and *ScS* ray paths for all source-receiver combinations from the actual data set. To do this, the reference model for the aspherical structure was adjusted from PREM to SYLO. We did not include *sS* paths in the calculations for the aspherical model due to the very strong shallow heterogeneity in the shear velocity model which poorly approximates the detailed structure near subduction zones.

The predicted differential travel time anomalies relative to model SYLO for downgoing phases are shown in Figure 7 for the same source-receiver geometries as in our data. The fast D" layer in model SKS12WM13 predicts large negative *ScS-S* anomalies across the region, but this is not consistent with the data. The pattern is almost unchanged if the PREM model is used as a background structure for computing the ray paths, but there is about a 1.5 s baseline shift in that case (model SYLO is slightly slower than PREM above the D" region, as apparent in Figure 3, over a depth range that has a higher velocity in model SKS12WM13). The pattern of *ScS-Scd* anomalies has some correlation with the data, with the most negative anomalies concentrating in the same area, but there is a significant baseline shift to too fast of an overall D" velocity (for a constant depth discontinuity), and the scale length of perturbations in the observations is not achieved by the model. The observed and predicted *Scd-S* anomalies agree in overall strength and general pattern, although again there is a baseline shift that appears to reflect the predicted *S* times not being fast enough (and/or *Scd* being too fast) in model SKS12WM13. It is notable that the region with the most uniform observation of the *Scd* phase corresponds to that with the largest predicted *ScS-Scd* travel time perturbations and fastest region of D" in Figure 7. This suggests that the volumetric model incorporates data that sample the same high-velocity structure that gives rise to the *Scd* phase but incorrectly distributes the anomalies due to the smooth model parameterization. Overall, some of the trends in the observations can be accounted for with model SKS12WM13, but use of this model to apply corrections for long-wavelength structure does not appear warranted, as there are significant baseline shifts and spatial inconsistencies that are likely to be due to limited resolution in the aspherical model. Higher-resolution tomographic models are becoming available, and in some cases, they do adequately match the direct *S* travel time anomalies because they have stronger midmantle heterogeneity [e.g., *Schwartz et al.*, 1991b; *Grand*, 1994]; however, the data in our study provide a more powerful means for assessing scales of lateral heterogeneity in the region of the D" discontinuity.

An alternative to using an aspherical model to correct for structure above D" is development of empirical source and station corrections for the differential times. For each event we can determine the mean value of the *Scd-S* anomalies and remove these averages from the data. The underlying assumption is that any mean term represents either the effect of near-source structure with a common effect on all stations (i.e., a depth mislocation effect, or common slab structure anomaly) or a common adjustment to the lower mantle reference model. It is also possible to compute mean station terms for all event-corrected data and to remove such terms from the data, assuming that these represent systematic ray parameter dependent path effects in the upper mantle under each station. Corrections such as these have been applied by *Thomas and Weber* [1996] in examining *P* wave velocity structure beneath Eurasia.

Figure 8 shows the results of removing event corrections and both event and station corrections from the *Scd-S* observations under Alaska. Only events and stations with at least 3 observations each were retained. As expected, the variance of the residuals is reduced relative to the uncorrected residuals in Figure 4, and the long-wavelength pattern under eastern Alaska is reduced. This procedure reinforces the interpretation that heterogeneity above D" causes much of the pattern in the *Scd-S* values, but it does not resolve where the structure is because the souce-receiver geometry is inadequate to separate near-source from midmantle effects. In fact, the number of observations is inadequate to reliably determine source and receiver corrections, as we found that application of this procedure to the larger *ScS-S* anomaly data set yields a tendency for the source and receiver terms to decrease with increasing number of observations. This means that the apparent improved fit of the reference discontinuity structure (as many residuals decrease toward zero) may give false con-

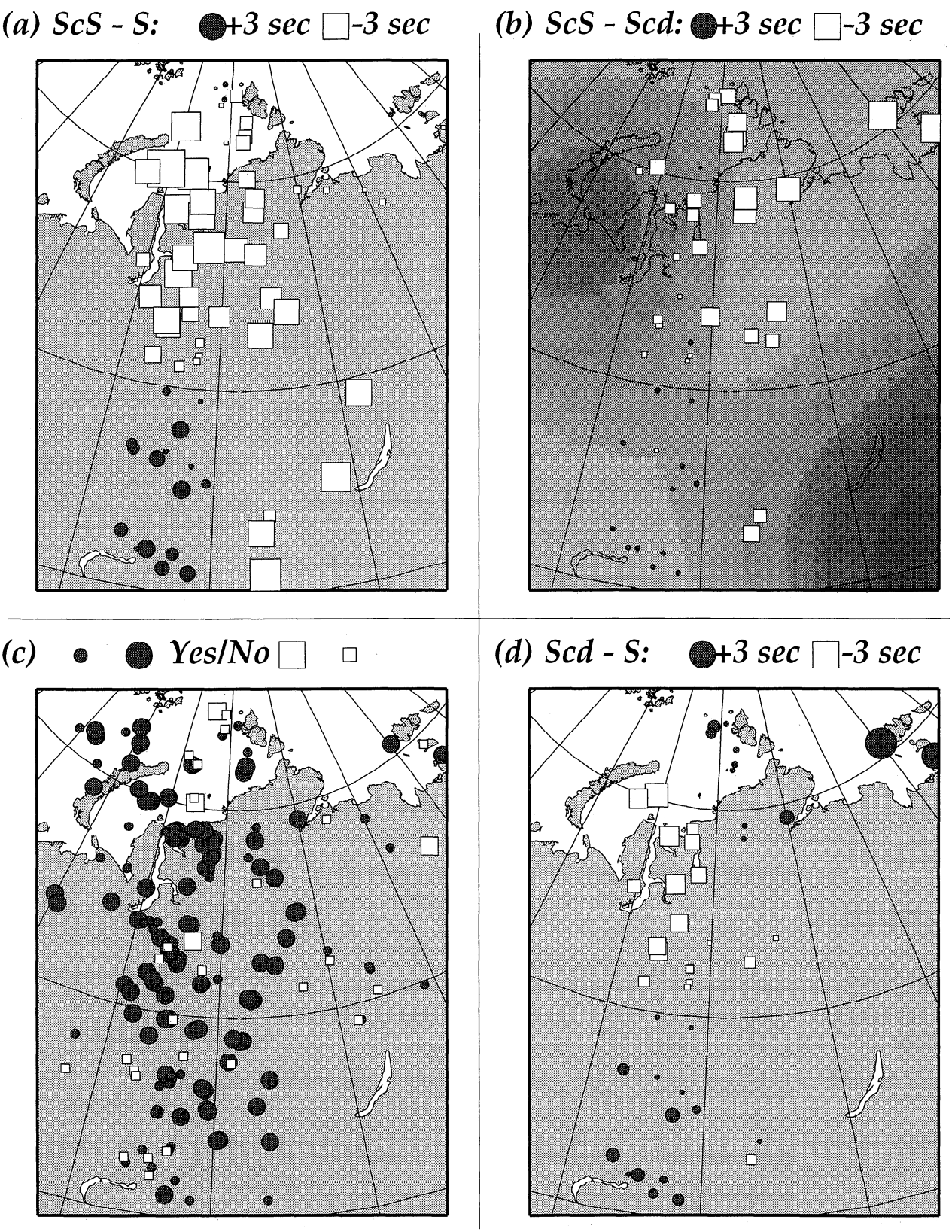

Figure 11. Predicted differential travel time anomalies for (a) *ScS-S*, (b) *ScS-Scd*, and (d) *Scd-S* using model SKS12WM13 corrected to have model SGLE as a reference structure for paths under Eurasia. Anomalies for surface-reflected phases are not included. The residuals are plotted at the *ScS* reflection point for each path. Anomalies with values of less than ±0.5 s are plotted with symbol sizes for values of ±0.5 s so that they are visible. (c) Map showing the midpoint of all paths in the data set of *Gaherty and Lay* [1992], indicating whether an *Scd* phase was observed (yes) or not (no) for each case where model SGLE would predict an observable phase. Two symbol sizes are used to indicate the confidence in the decision about whether *Scd* is present, with larger symbols reflecting higher confidence one way or another. In Figure 11b, the lateral shear velocity structure at a depth of 2800 km in the model of *Liu and Dziewonski* [1994] is indicated by shaded contours in 0.5% increments ranging from 0.0 to -0.5% slow (lightest shading) up to more than 2.0% fast (darkest shading).

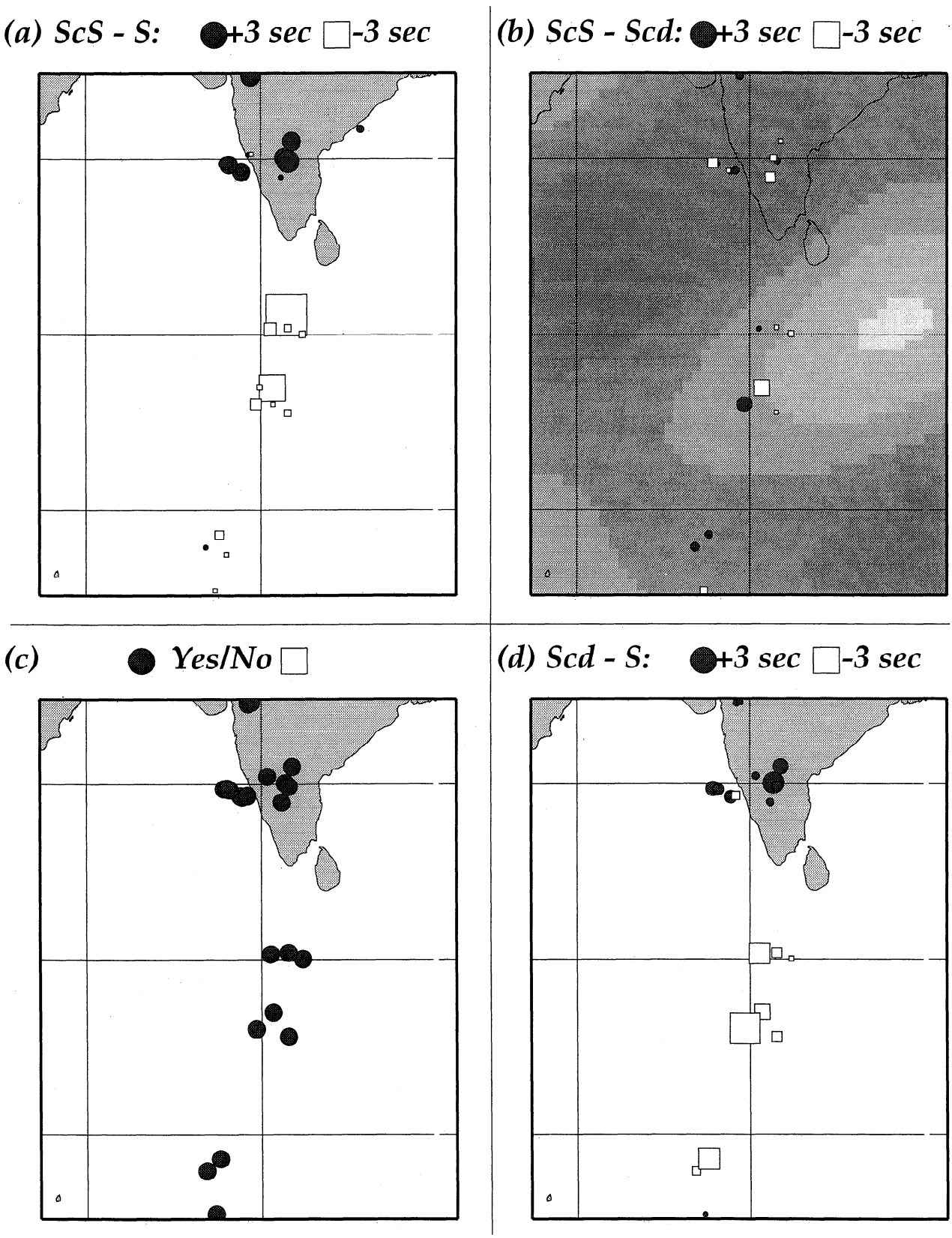

Figure 12. Differential travel time anomalies for (a) *ScS-S*, (b) *ScS-Scd*, and (d) *Scd-S* relative to model SYL1 for paths under India and the Indian Ocean. Anomalies for surface-reflected phases are included. The residuals are plotted at the *ScS* (or *sScS*) reflection point for each path. Anomalies with values of less than ±0.5 s are plotted with symbol sizes for values of ±0.5 s so that they are visible. (c) Map showing the midpoint of all paths in the data set of *Young and Lay* [1987b], indicating whether an *Scd* phase was observed (yes) or not (no) for each case where model SYL1 would predict an observable phase. In Figure 12b, the lateral shear velocity structure at a depth of 2800 km in the model of *Liu and Dziewonski* [1994] is indicated by shaded contours in 0.5% increments ranging from more than -1.5% slow (lightest shading) up to more than 0.5% fast (darkest shading).

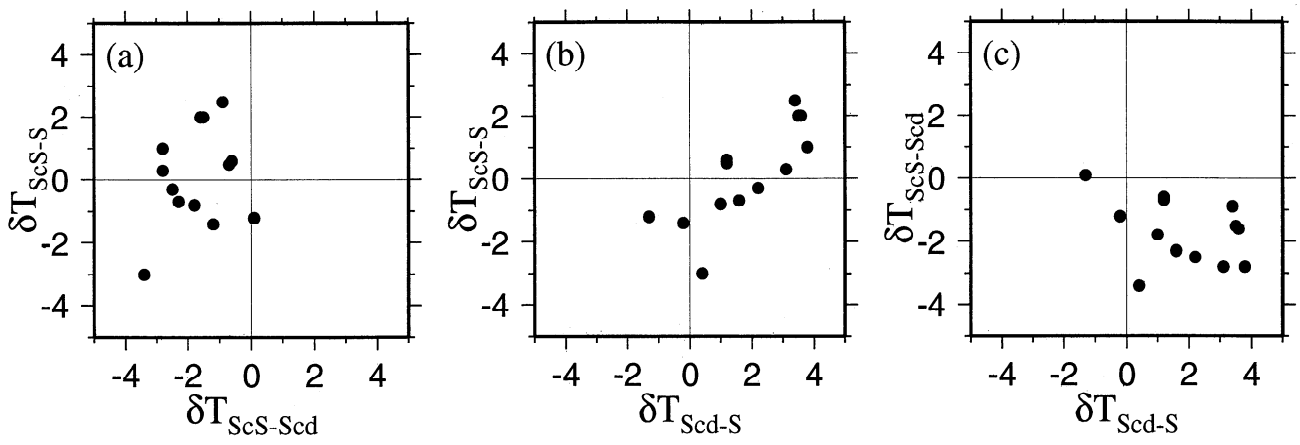

Figure 13. Scatterplots indicating the correlations between differential time anomalies for the direct phases sampling the mantle under India. (a) Differential anomalies with *ScS* in common. (b) Differential anomalies with *S* in common. (c) Differential anomalies with *Scd* in common.

fidence in the accuracy of that structure. The source and station corrected *Scd-S* anomalies do not show a stronger anticorrelation with the *ScS-Scd* anomalies in Figure 4 than for the uncorrected case, so it is likely that some true *Scd* variation is being suppressed. The application of such corrections is problematic for the relative differential anomaly procedure used in Figure 5 and should not be significant for *ScS-Scd* anomalies due to their very similar near-source and near-receiver ray paths (see Figure 1), so we do not pursue it further. It is clear that the differential times in Figure 4 are affected by some superimposed scatter induced by actual near-source and near-receiver heterogeneity, so we rely on general trends in the data for our interpretations.

The differential travel time anomalies for paths under Eurasia are shown in Figure 9, along with a plot of yes/no indicators of whether *Scd* was observed on various seismograms [*Gaherty and Lay*, 1992]. *Gaherty and Lay* [1992] considered these patterns in some detail. The pattern of *S* wave velocity heterogeneity in model SKS12WM13 is again superimposed on the *ScS-Scd* plot. This region has a relatively fast D" layer in model SKS12WM13. The relative behavior of the residuals is quite similar to that beneath Alaska. The *ScS-S* anomalies are strong, ranging over 6 s, with systematic spatial patterns with a scale length of 500-1000 km. This is very similar to the *Scd-S* anomaly pattern, strongly suggesting that the origin is not within D". The *ScS-Scd* fluctuations, which provide the best localized sampling of D", show smaller-scale variability and a somewhat lesser range of residuals than for the other phase combinations. There is again no simple relationship between *ScS-Scd* anomalies and the regions where *Scd* phases are more erratically observed. Note the interesting pattern of alternating positive and negative anomalies trending north-south in the *ScS-S* and *Scd-S* residuals in Figure 9. These are spaced at about 9 degrees separation, or of the order of 500 km and appear to be unrelated to the *ScS-Scd* scatter. If these are a manifestation of thermal heterogeneities affecting direct *S*, they may correspond to small scale upwellings and downwellings in the deep mantle around 500 km above the CMB under Eurasia. Such small-scale features are not revealed by the current generation of global models, as shown below.

The correlations between these residuals are apparent in the scatterplots in Figure 10, with the linear correlation coefficient being strongest for *ScS-S* and *Scd-S* (0.76), moderate for *ScS-Scd* and *Scd-S* (-0.44), and weak for *ScS-S* and *ScS-Scd* (0.24). The surface-reflected phases are rather sparse in this region and correlations are not shown for these phases. The most straightforward interpretation is that there are again strong variations in direct *S* times, which span about 5 s anomalies. *Gaherty and Lay* [1992] drew this conclusion as well. At the very least, much of the travel time anomaly common to the *ScS-S* and *Scd-S* patterns arises from structure above the D" region. *Scd* fluctuations are responsible for most of the scatter in the *ScS-Scd* anomalies. While there is likely to be some heterogeneity within the D" layer which affects only the *ScS* times, the scatter introduced by this structure appears to be weaker than that separately affecting *S* and *Scd*.

Differential time anomalies predicted by ray tracing through model SKS12WM13, corrected to a reference structure given by SGLE, are shown in Figure 11. Comparison with Figure 9 reveals that the model predicts relatively little of the observed patterns, and the observations contain significant coherent small-scale structure that is not predicted by the tomographic model. The range of residuals is underpredicted in each case as well, by about a factor of 2. The mismatch is not unexpected, given the heavy smoothing intrinsic to the large scale tomographic model, but it does indicate that use of the additional differential time measurements including *Scd* arrivals is likely to improve the resolution of future tomographic modeling efforts. While the tomographic model predicts some rather rapid spatial gradients in point-wise anomalies (in part, due to differing path geometries through the region with common midpoints), the range and spatial gradients in the anomalies are greater in the data, suggestive of small-scale structure in the boundary layer.

The third data set is displayed in Figure 12, with the differential time anomalies for paths under India being shown. The behavior of the differential times corresponds well with that in other regions, with similar patterns in the anomalies involving direct *S*, and weaker anomalies in the D" sensitive measures, *ScS-Scd*. The sampling is limited due to the

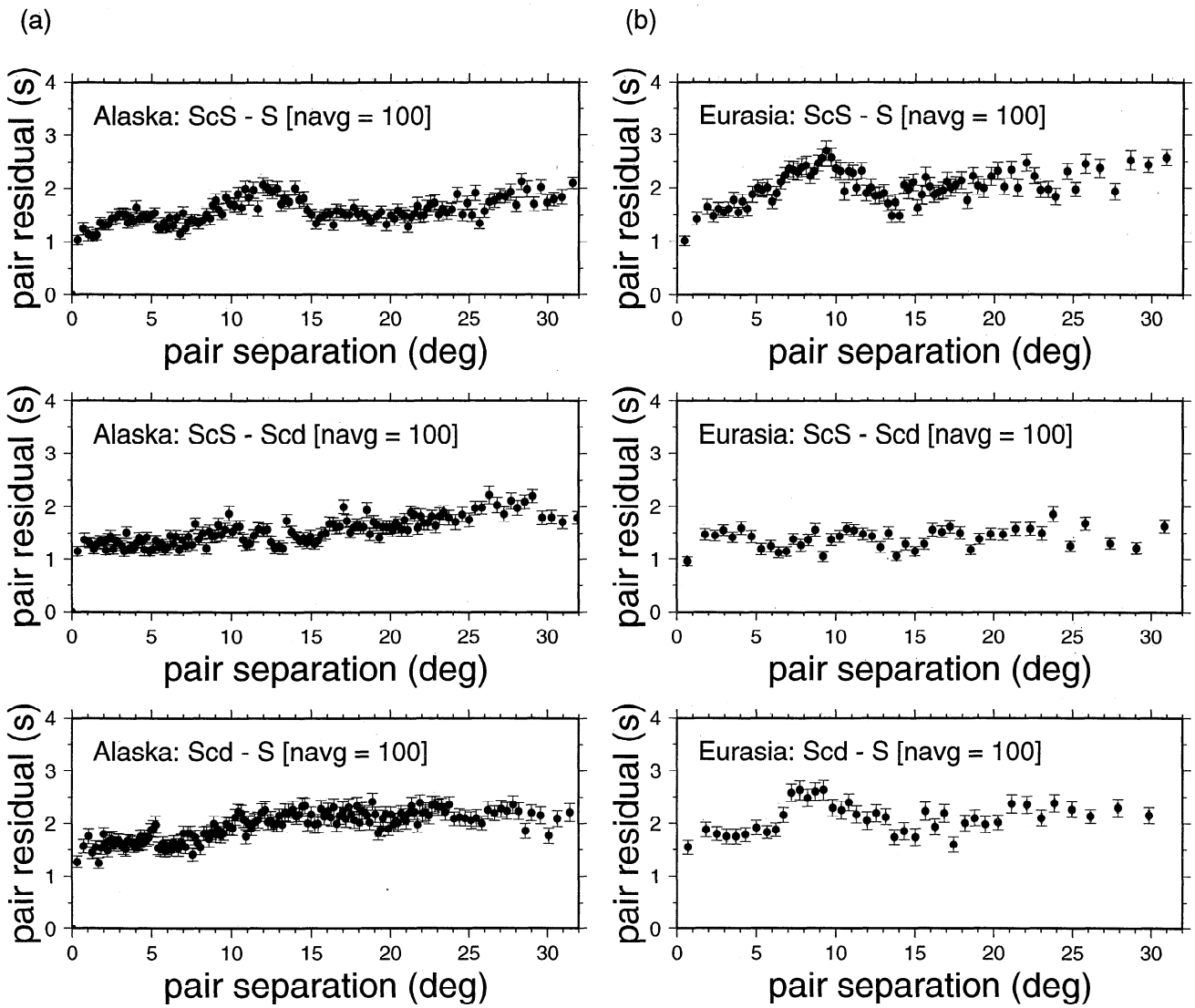

Figure 14. Spatial characteristics of the residual patterns for *ScS-S*, *ScS-Scd*, and *Scd-S* for (a) Alaska, (b) Eurasia, and (c) India. The absolute value of the difference between each pair of residuals is plotted as a function of the separation distance between their *ScS* reflection-points, and a running mean is computed in groups of 100 (for Alaska and Eurasia) or 10 (for India). The vertical error bars indicate the standard error of the mean in each bin, and the horizontal error bars (only visible in Figure 14c) indicate the standard error in the distance range used in each bin. Peaks suggest spatial separations with stronger heterogeneity.

source/receiver geometry for distances appropriate to observe *Scd*, but the general pattern in the *ScS-S* anomalies is consistent with the larger data set analyzed by *Lavely et al.* [1986], in which negative anomalies were found in the central Indian Ocean region. There is a trend from south to north for both *ScS-S* and *Scd-S* residuals which indicates a common origin in the direct *S* phases. *Lavely et al.* [1986] argue that *ScS* times are better correlated with *ScS-S* differential anomalies than *S* times for paths under the Indian Ocean and conclude that the primary heterogeneity resides in D", but our results throughout this paper contest this as a general inference, at least for the regions we consider in detail. Model SKS12WM13 predicts lateral variations in D" structure in this region, as shown in Figure 12, but the model does a poor job of predicting any of our observations (the trends in the observed and predicted residuals are anticorrelated), so it appears that this is a poorly resolved part of the global model.

The correlations between the differential anomalies for the paths under India and the Indian Ocean are shown in Figure 13. The residuals are somewhat baseline-shifted relative to model SYL1, because many of the observations used to constrain that model were from larger distances where *Scd* is not an isolated arrival. Nonetheless, the correlation is strong for *ScS-S* and *Scd-S* (0.80), weak for *ScS-S* and *ScS-Scd* (0.28), and moderate for *ScS-Scd* and *Scd-S* (-0.36). The general tendencies are the same as for the two other data sets, with strong variations in the direct *S* times and relatively weak contributions from the D" layer itself to the *ScS* times.

Scales of Heterogeneity

Given the limited spatial sampling provided by our data and the lack of crossing ray coverage, it is not viable to invert for a tomographic model from which the heterogeneity

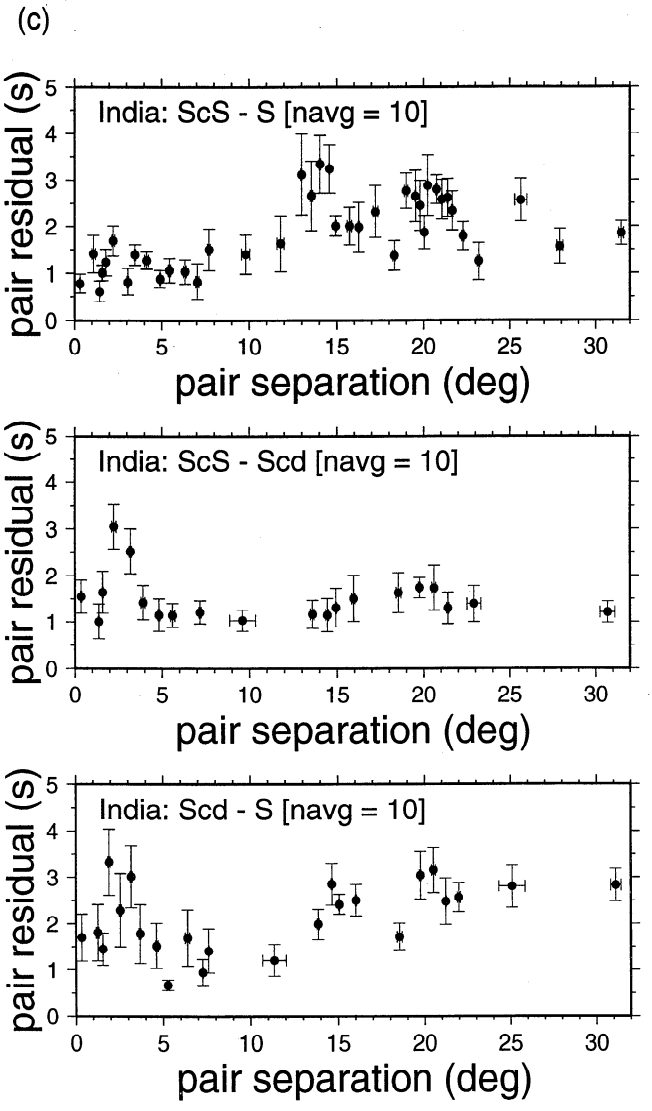

Figure 14. (continued)

power spectrum may be inferred. Such procedures tend to involve heavy smoothing as well and probably underpredict the small-scale structure, so we constrain our analysis to the data as much as possible. A useful procedure for assessing the structure in our sparse, nonuniform path coverage is the method introduced by *Lavely et al.* [1986], which approximates a spatial autocorrelation function of the residual patterns. *Gaherty and Lay* [1992] previously applied this method to the Eurasian differential times, and we consider all three data sets here for ease of comparison. A moving average is computed for the absolute value of the residual difference as a function of distance of separation between the *ScS* reflection points for each pair of observations in a given region. For N travel time differentials, there are $N(N-1)/2$ differences sorted by distance. For the Alaska and Eurasia data sets, which are relatively dense, the averaging is done in groups of 100, while it is done in groups of 10 for the Indian data set. The resulting spatial characteristics of the differential times are shown in Figures 14a, 14b, and 14c for Alaska, Eurasia, and India, respectively.

The Alaska *ScS-S* differential times (Figure 14a) show minor peaks around 4° and 12°. The *ScS-Scd* autocorrelation is quite flat at short scale lengths, indicative of small-scale heterogeneity, while the *Scd-S* spectrum has a broad peak centered around 15°. These features are consistent with the visual trends in Figure 4. There is some suggestion of long-wavelength trend indicated by the general increase across the separation range, and this is consistent with the results of similar treatment of the anomalies predicted by model SKS12WM13. Our data cannot bound the larger scale heterogeneity, but it is clear that the strength of heterogeneity is not dropping off precipitously at the shorter scales, so any assertion that the heterogeneity spectrum is very red in the deep mantle is not supported by our data. The Eurasian differential times (Figure 14b) show sharper peaking at 8-9° separations for *ScS-S* and *Scd-S*, but again a relatively flat *ScS-Scd* autocorrelation with minor peaks at 3°, 11°, 17° and 22°. These patterns reinforce the argument that there is significant power in the *S* velocity heterogeneity at scale lengths of 600-1000 km in these regions, and it is not concentrated in the D" layer. The India data are rather sparse, so the autocorrelation is less stable, but the large-scale trend of the *ScS-S* residuals across the region is manifested in the peak at 14° and 20° in Figure 14c. In this case *ScS-Scd* shows a relative peak at horizontal scales of 2-3°, and there is a similar feature in the *Scd-S* anomalies. The vertical axis intercepts of these curves suggest a precision of about 1 s in the observations, but this is a point-wise measure, which neglects the actual finite path length associated with each anomaly. The behavior for all three regions suggests that significant D" heterogeneity exists at smaller scales and that it results in less pronounced (path-integrated) velocity anomalies than does the mid-lower mantle.

Ideally, extensive crossing ray coverage is available to sort out the larger scale heterogeneity affecting the direct *S* phases in order to remove resulting trends from the data. However, our coverage is inadequate to do this stably, and we have seen that existing aspherical Earth models are probably not sufficiently reliable at present to provide corrections. We recognize the potential bias of inferring point-wise fluctuations of velocity structure, so we conduct several analyses that include the extended path length of the phases in our differential measurements. This requires some assumptions about the depth extent over which anomalies accumulate. Figure 15 illustrates the finite path length effects for *ScS-S* differential anomalies under Alaska. The anomalies are converted to shear velocity perturbations over a path length corresponding (arbitrarily) to the length of the *ScS* path within a 250 km thick D" layer. The grazing geometry makes the path lengths in D" rather extensive. The paths with varying percent velocity anomaly are subdivided into four groups that are shown separately. There is a spatial pattern with the more negative perturbations (slower *ScS* times or faster *S* times) in the center of the sampled regions and the more positive perturbations on the margins. There is clearly some overlap in path anomalies but insufficient crossing coverage to localize the structure. The difficulty is exacerbated by the fact that the anomaly is likely to primarily be in the *S* phases, which have different turning depths. The finite path effects do not modify the basic argument that there are intermediate (500-1000 km) scale heterogeneities affecting these data, but the strength of the velocity perturbations depends on how the anomaly is distributed (and which phase it is attributed to). It is clear that ±1.5% veloc-

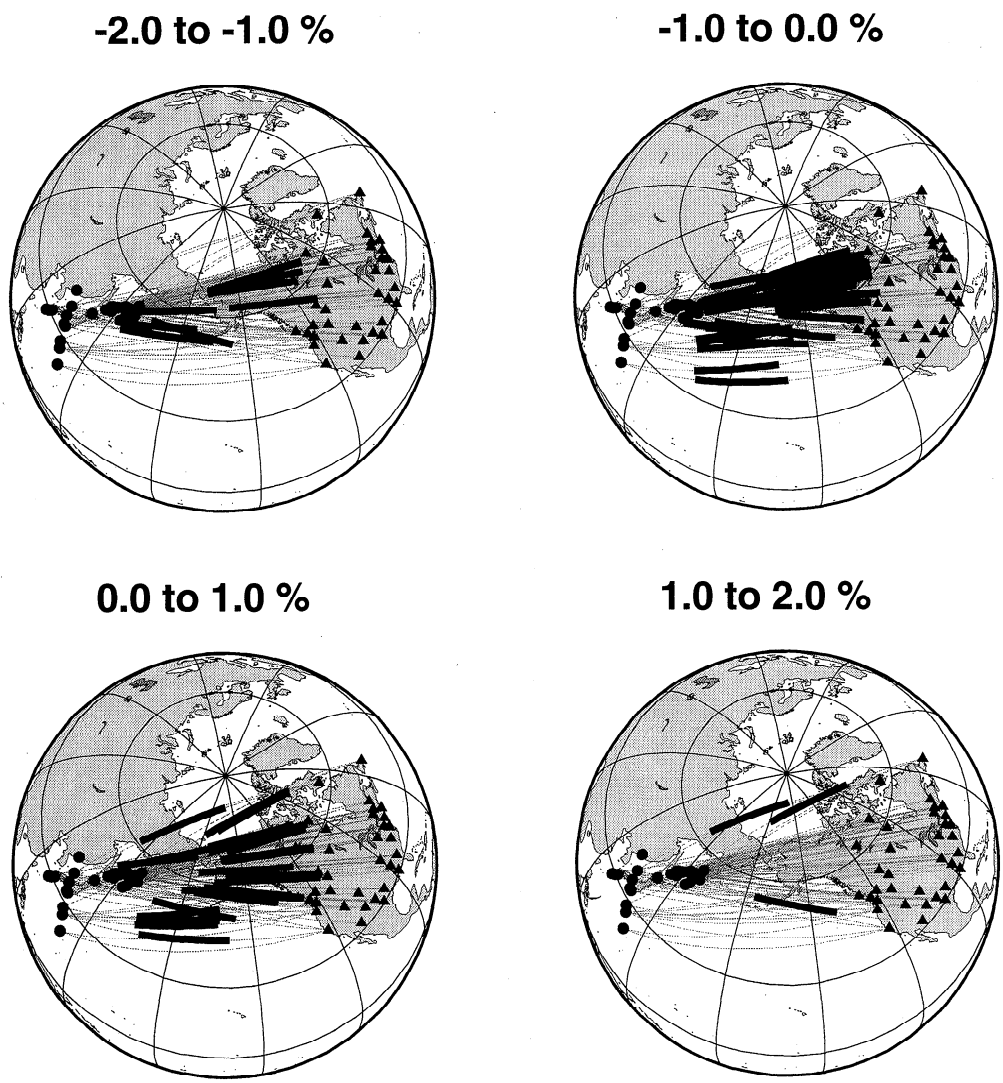

Figure 15. The actual path coverage for differential time measurements under Alaska, with the portions of the *ScS* paths located within a 250 km thick D" region being darkened. The paths are grouped into subsets with different inferred uniform velocity perturbation along each path, ranging from -2% to +2%, based on the assuming the *ScS-S* anomalies are localized to the D" region.

ity fluctuations are likely to exist in the lower mantle in this region with scale length of about 750 km and depths 300-600 km above the CMB. This is compatible with features under North America in the high-resolution shear wave tomography model of *Grand* [1994], but with our coverage it is difficult to extract more information from the *ScS-S* anomalies.

Interpretation of the *ScS-Scd* anomalies is somewhat less ambiguous mainly because these phases have more proximate turning points (Figure 1) and intrinsically less sensitivity to shallow mantle heterogeneity. For these residuals, the major issue is whether the anomaly fluctuations arise from volumetric heterogeneity within D" or from topography of the discontinuity that gives rise to the *Scd* phase. The clearest indication we have as to the cause of the fluctuations is the relatively strong correlations that are observed between *ScS-Scd* and *Scd-S* anomalies (Figures 5 and 10), which indicate that the patterns are largely due to *Scd* variations rather than *ScS* variations. The indicated variations in *Scd* times are about 4 s, which is very large, as it must accumulate within the relatively localized region where *Scd* and *ScS* paths diverge at the base of the mantle. Another important piece of information is that the heterogeneity in *Scd* exhibits rapid lateral variations (Figures 4 and 9) with stronger gradients than predicted for a smooth aspherical Earth model like SKS12WM13 (Figures 7 and 11). The autocorrelations for *ScS-Scd* anomalies are relatively "white", with minor peaks around 2-3° (Figure 14). As discussed earlier, the *Scd* phase only penetrates a few tens of kilometers into the top of the D" layer at the distances of our data, which together with the rapid lateral variations, suggests that any volumetric heterogeneity is concentrated in a rather thin layer at the top of D" or there is a corresponding topography on the boundary with higher regions (shallower discontinuity) corresponding to regions in the volumetric model with larger *ScS-Scd* differential time anomalies.

Assuming that the *ScS-Scd* anomalies accumulate within a 50 km thick layer at the top of D" (with no topography on the boundary), the differential time anomalies are mapped

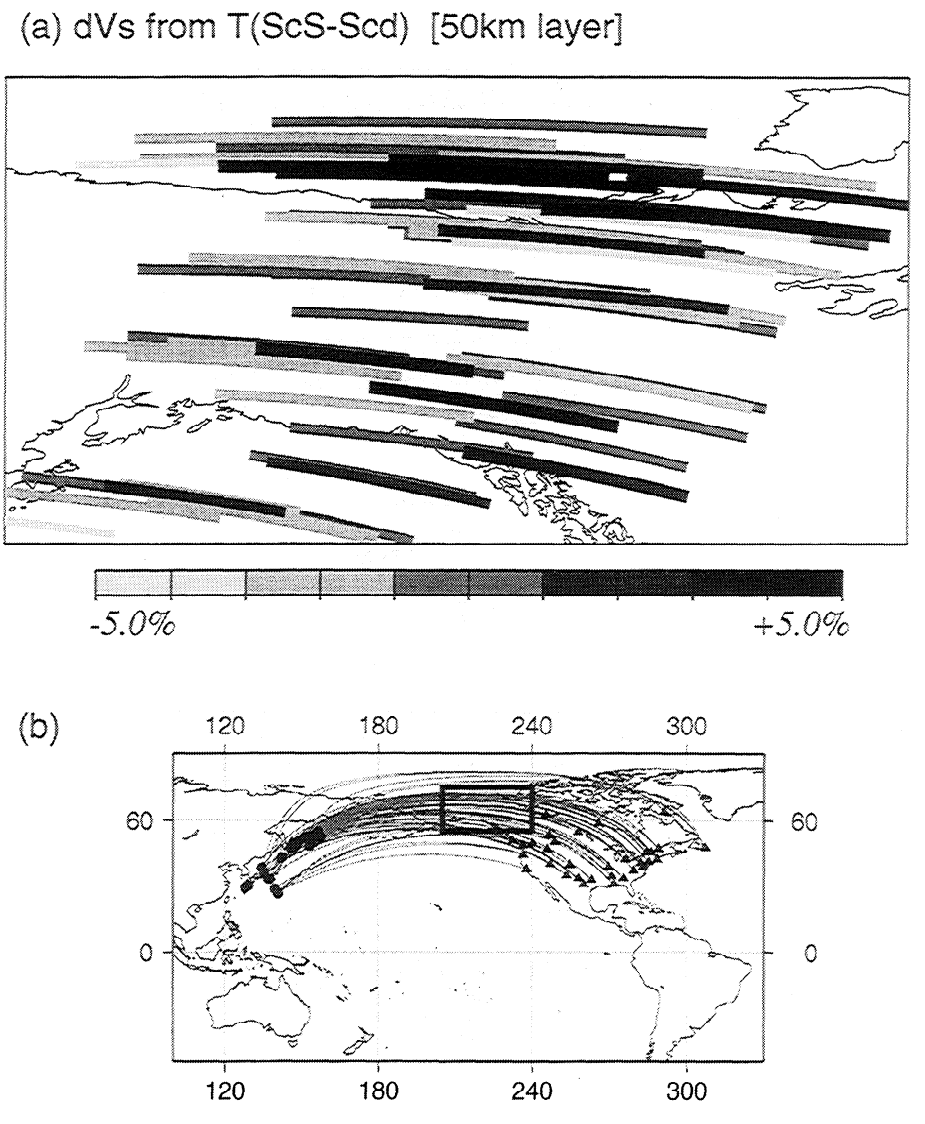

Figure 16. (b) The actual path coverage for *ScS-Scd* differential times beneath Alaska. (a) The path segments corresponding to the length of path in which *Scd* is in a 50 km thick region at the top of the D" layer. The same path length is assumed if the anomaly is attributed to *ScS*. The differential time anomalies are converted to percent shear velocity perturbation along that path length assuming that all of the anomaly is due to volumetric structure encountered by *Scd* (or by reversing the scale, to volumetric structure encountered by *ScS*). For scale, the vertical width of Figure 16a is about 1200 km at the core-mantle boundary. The map projection distorts the path lengths at the highest latitudes.

into percent velocity variations along the *Scd* path through the layer, and plotted on the corresponding ray path segment in Figure 16 for Alaska and Figure 17 for Eurasia. The lack of crossing ray coverage is particularly evident in these plots and prevents any tomographic reconstruction of the heterogeneity, but viewing the path coverage is useful for revealing the small-scale heterogeneity implied by these anomalies. In Figure 16, the nearly parallel paths under Alaska show close proximity between paths with several percent inferred velocity heterogeneity. The streaking of the paths allows for some spatial separation not accounted for in the midpoint structure of the autocorrelation, but it appears that ±4% heterogeneity is still required with lateral scales of several hundred kilometers to account for these data. We certainly expect the Fresnel zone averaging of the long-period *S* phases to smooth over the true heterogeneity, and some of the scatter results from accumulated path anomalies above the D" region, but it is very likely that concentrated small-scale heterogeneity at the top of D" is responsible for a significant portion of these differential travel time anomalies. The same conclusion can be drawn for the paths under Eurasia (Figure 17), where there is somewhat better ray path crossing coverage and a clearer separation of fast and slow regions. The strong lateral fluctuations near the northern coastline of Eurasia correspond to a region with intermittent observations of short-period *P* wave reflections from D" [*Weber and Davis*, 1990; *Weber*, 1993], and it may be that the *S* wave structure is somewhat more coherent or that our long-period data are averaging over a structure that is truly intermittent spatially. It is important to note that such

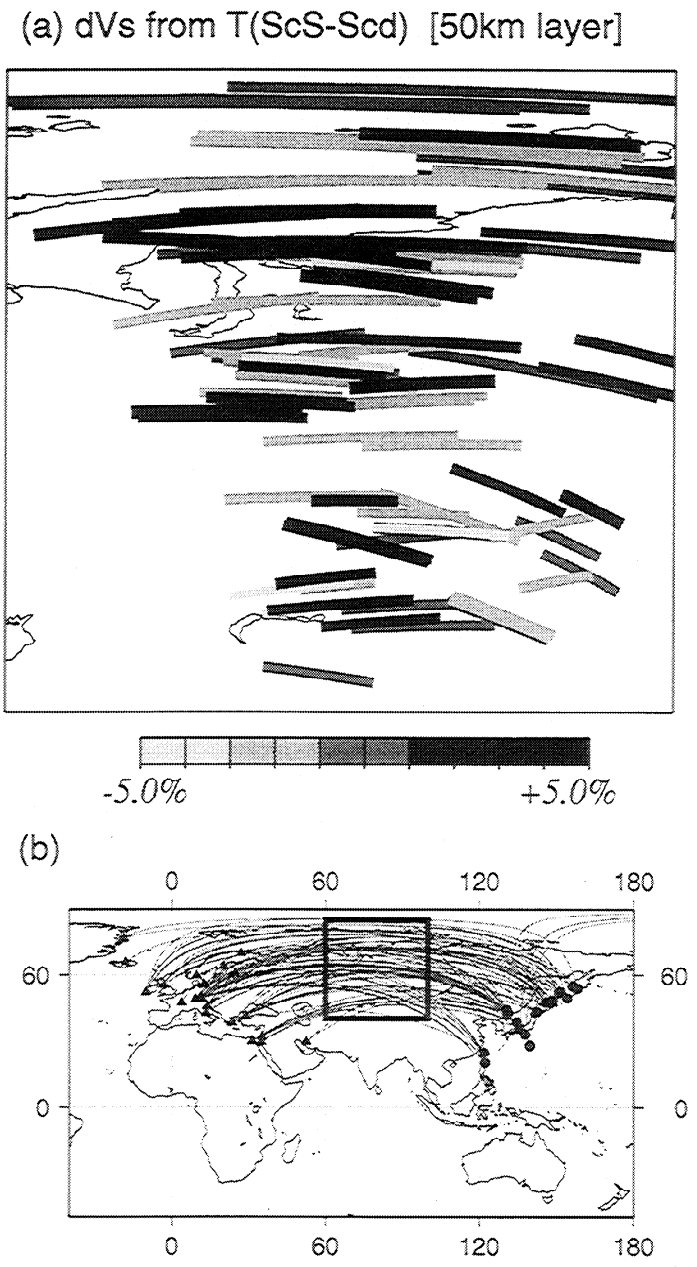

Figure 17. (b) The actual path coverage for *ScS-Scd* differential times beneath Eurasia. (a) The path segments corresponding to the length of path in which *Scd* is in a 50 km thick region at the top of the D" layer. The same path length is assumed if the anomaly is attributed to *ScS*. The differential time anomalies are converted to percent shear velocity perturbation along that path length assuming that all of the anomaly is due to volumetric structure encountered by *Scd* (or by reversing the scale, to volumetric structure encountered by *ScS*). For scale, the vertical width of Figure 17a is about 3100 km. The map projection distorts the paths lengths at the highest latitudes.

strong lateral heterogeneities could locally obscure or eliminate the discontinuity itself, which is only 2.75% on average, while making it much stronger in other areas. This may be consistent with the intermittent nature of the structure revealed in shorter-period energy and in *P* waves.

Rather than attributing the *ScS-Scd* differential time anomalies to volumetric heterogeneity within the upper portion of D", one can infer topography on the boundary. Using one-dimensional ray tracing to map the differential times into topographic relief yields lateral variations of ±50 km in both the Alaska and Eurasia regions, where we perturb only the *Scd* time. Positive velocity perturbation regions (for *Scd*) in Figures 16 and 17 would correspond to regions with a shallower discontinuity. This mapping is more ambiguous than for volumetric heterogeneity, given that it is unclear how the velocity model within D" should change with the topography and whether or not the *ScS* paths should be affected. The inferred topography, which gives rise to 4-5 s fluctuations in *Scd* arrival times, is rather acute, given the several hundred kilometer scales that are indicated, and one-dimensional ray paths are undoubtedly incorrect. Waveform modeling with reflections from an undulating

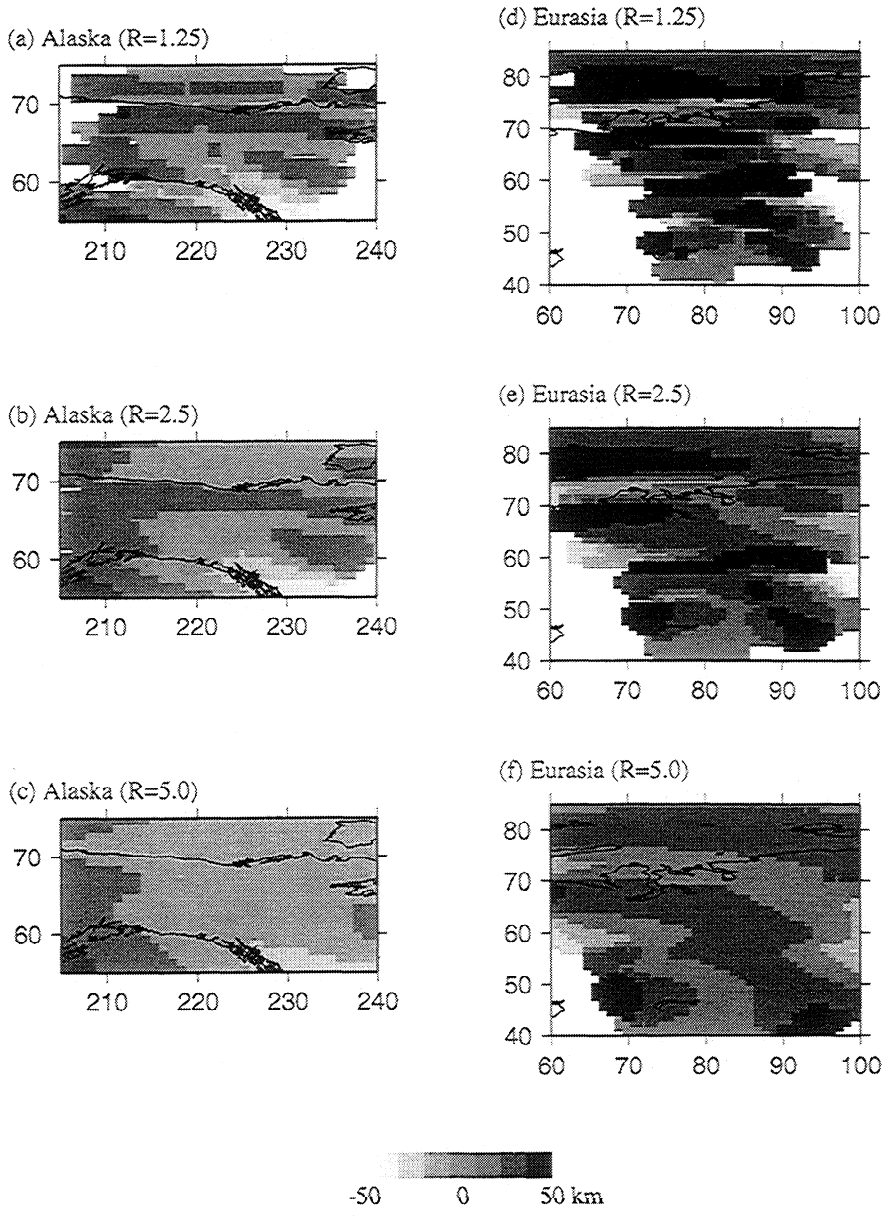

Figure 18. Gaussian cap-averaged mapping of *ScS-Scd* anomalies into D" topography for paths under (a) Alaska, with a cap radius of 1.25° using the weights described in the text, (b) Alaska with a 2.5° cap and the same weights, (c) Alaska, with a 5° cap and the same weights, (d) Eurasia with a cap radius of 1.25°, (e) Eurasia with a cap radius of 2.5°, and (f) Eurasia with a cap radius of 5°.

boundary may be worth pursuing as the data coverage expands, but we feel that this should be performed with broadband data, for which small waveform details may help to guide the modeling, rather than the long-period data used in this study. As we expect significant wave front healing effects to obscure the small-scale topographic irregularities, it will be very challenging to invert for a sensible model of topography.

It is likely that if small-scale topography is present in the D" discontinuity, it is accompanied by volumetric heterogeneity on both sides of the boundary. The apparent small-scale structure of the differential time anomalies in Figures 16 and 17 is likely to be the result of a combination of both topography and volumetric heterogeneity. Indeed, if the boundary is itself the upper side of a rubble zone of chemically and thermally heterogeneous material, it is possible that it has structure at many scale lengths, which are averaged over by the Fresnel zone of our data set. We produce one more projection of the *ScS-Scd* differential time anomalies, with a spatial filter to bring out the larger-scale structure. For the Alaskan data we use data quality assessments that were assigned to each *Scd* measurement by *Lay and Young* [1996] as weighting factors in combining the data. The quality measures (1 is poor and 4 is excellent) are mapped into weighting factors, which are then used in running a cap average over the Alaska *ScS-Scd* ray path sampling where we assume the *Scd* encounters topography over the path lengths shown in Figure 16. For the Alaska

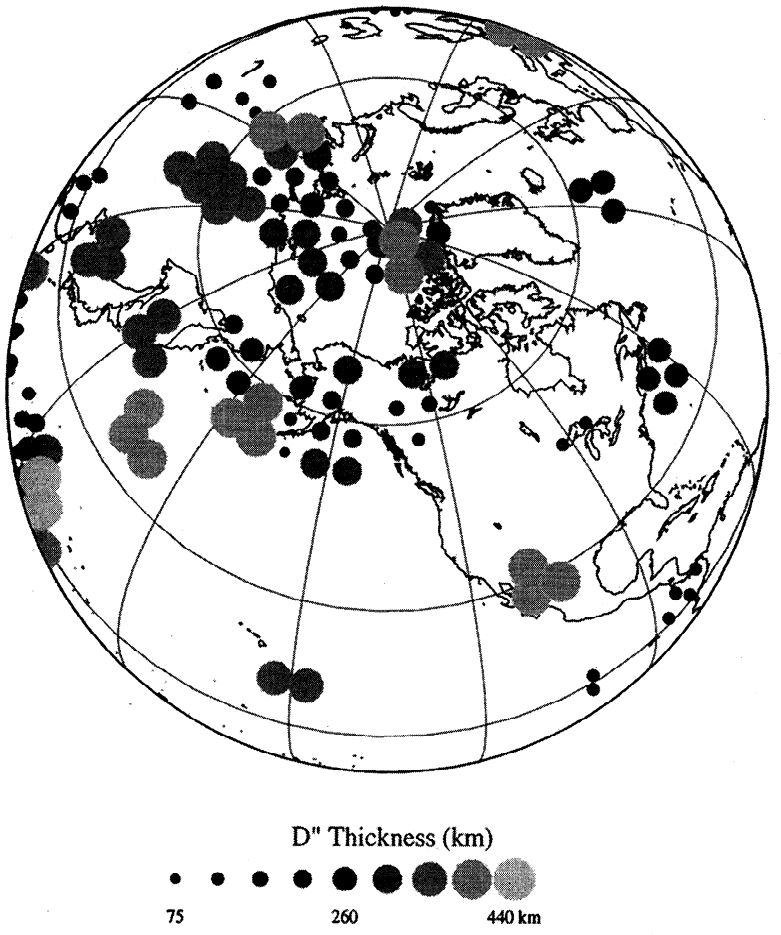

Figure 19. Estimates of the thickness of D" (distance from the CMB to the top of the shear velocity discontinuity) from *Sbc* reflections in the study of *Kendall and Shearer* [1994]. Their point estimates have been averaged with a 5° cap average. Note the lateral fluctuations of ±100 km suggested by their global data and the strong variations inferred for the regions under Alaska and Eurasia. The patterns in Figure 18 can be compared with these results which are from a much sparser data coverage in the same areas.

region, Figures 18a, 18b, and 18c shows the Gaussian cap-averaged topography for cap radii of 1.25°, 2.5°, and 5°, respectively. Similar results for Eurasia are shown in Figures 18d, 18e, and 18f, with no weighting factors. The effective Fresnel zone for these data is between 1.25 and 2.5°, so the more heavily smoothed plots are most reliable. The Eurasian region shows more pronounced topographic fluctuations relative to the mean structure, as expected from Figure 17. The smoothing provided by the cap averaging is not necessarily the same as would emerge from tomographic reconstruction but does filter out the more rapid spatial variations that are likely to result from combined topography/volumetric heterogeneity fluctuations. Topography of several tens of kilometers over lateral scale lengths of 200-500 km is indicated for both regions, although this is not uniquely resolved from volumetric heterogeneity. In fact, the topography calculation is very simplified and for finite frequencies is likely to prove quite different from this simplified analysis.

Discussion and Conclusions

Other efforts to map out lateral variations in lowermost mantle shear velocity structure are yielding results generally comparable to the features in this study. For example, *Kendall and Shearer* [1994] used *Sbc* reflections from the D" region to image lateral variations in the depth of the discontinuity, finding significant fluctuations under both the Alaska and central Eurasia regions. The 5° cap-averaged values of D" thickness in the northern hemisphere from their study are shown in Figure 19. There is reasonable consistency in the spatial patterns in Figures 18 and 19, although the overlap in coverage is limited. For example, we find a somewhat thicker D" region in north Alaska and under the Gulf of Alaska, as is also seen in Figure 19. We also detect a region of very thin D" just north of the Eurasian coastline, where they find thinner D" as well, and where *Weber* [1993] has documented strong lateral variations. *Kendall and Shearer* [1994] observe fluctuations in these two subregions comparable to those found on a global basis, whereas we find less pronounced variations in the subregions. In part this may reflect the greater stability of *Scd* phases, which are enhanced by critical angle amplification relative to *Sbc*. In addition, both approaches are unable to resolve the trade-off between topography and volumetric heterogeneity within D". Nonetheless, the results do agree in that they indicate lateral fluctuations in the discontinuity structure over the scale of the subregions, requiring 500 km and smaller-scale heterogeneity. This is consistent with the results of many

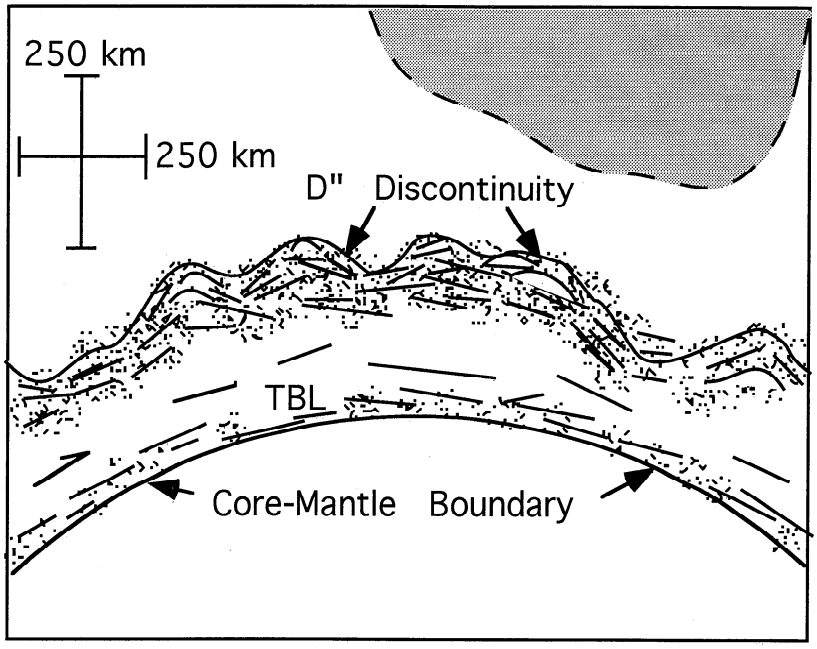

Figure 20. A cartoon summarizing the general characteristics of the lower mantle regions sampled in this study. Relatively large-scale lower mantle heterogeneities affect direct *S* waves, while moderate- and small-scale structures affect *Scd* times. *ScS* turns in a relatively homogeneous D" layer with a thermal boundary layer (TBL) right above the core-mantle boundary. The discontinuity at the top of D" has lateral coherence over regions of the order of 1000 km in lateral scale but significant small-scale fluctuations of topography (±50 km) and volumetric heterogeneity in the upper portion of D" (±4%). Shearing of the small-scale heterogeneity appears to induce anisotropy in the vicinity of the discontinuity, and this may also occur within the TBL.

studies of both *P* and *S* reflections from D" listed in the Introduction.

Lay and Young [1991] and *Garnero and Lay* [1997] have mapped shear wave anisotropy in the D" region beneath Alaska, finding that it can be effectively parameterized as transverse isotropy with *SH* motion traveling slightly faster than *SV* motion. They also find that the magnitude of transverse isotropy causing *SV/SH* splitting increases from near zero under the Aleutians to a maximum of 1.5% under eastern Alaska, basically corresponding to the region shown in Figure 16. *Garnero and Lay* [1997] argue that the anisotropy is linked to the shear wave discontinuity, with the discontinuity being weaker for *SV* waves by an amount corresponding to the extent of anisotropy. Their modeling cannot resolve whether the magnitude of anisotropy decreases within the D" layer, but that is certainly possible. The process responsible for producing anisotropy at the top of D" is unclear but is likely to be coupled to the process that accentuates the general heterogeneity in this region. Since the observations can be adequately accounted for by invoking transverse isotropy, there should be no affect of anisotropy on this study, as all differential times are between *SH* polarized arrivals.

New methods for imaging the three-dimensional structure using wave field migration [*Lay and Young*, 1996] and generalized double-beam methods [*Krüger et al.*, 1996] are advancing the strategies for differential travel time analyses beyond the great-circle assumptions made in this paper, but there is a shortage of three-component array data for assessing off great circle scattering from D" for *S* waves. Use of regional broadband array data holds promise for such applications, at least for longer period signals. At present, we are still a long way from having enough information to construct three-dimensional models or even two-dimensional models for the region by anything other than ad hoc parameterizations. Efficient algorithms for computing the two-dimensional wave fields encountering D" are being developed and will eventually play a role in quantifying the structure in D" [e.g., *Weber*, 1993; *Igel and Weber*, 1996; *Helmberger et al.*, 1996].

The overall result of this study favors a model with a D" region that is very heterogeneous in the depth range 150-300 km above the CMB, with several percent velocity heterogeneity in this region and/or ±50 km of topography on the shear velocity increase at the top of the region (Figure 20). It is possible that chemically distinct components of downwelling slabs, involving the old oceanic crust, contribute to the stronger heterogeneity in the vicinity of the discontinuity. This may in turn be related to the larger scale (>500 km) heterogeneities in the midmantle above the D" region that cause the large effects on direct *S* waves. Anisotropy develops in the upper portion of D", affecting the discontinuity structure, possibly as a result of shearing of small-scale structures near the discontinuity. The reduced fluctuation in *ScS* residuals relative to *S* and *Scd* indicates that the deeper portion of D" may be relatively homogeneous in structure, which may be the result of the smoothing effects of high temperatures in the thermal boundary layer right above the CMB. The increase in temperature and reduction of viscosity of the lowermost region of D" could actually reduce the velocity heterogeneity over a region on the lateral scale of 1000-2000 km. The lower temperatures, higher viscosity, and perhaps chemical heterogeneity of the upper portion of D" may be responsible for sustaining the

strong heterogeneity near the D" discontinuity. The recent evidence favoring a thin ultralow velocity region at the base of D" in areas of hotter than average mantle [e.g. *Garnero and Helmberger*, 1995, 1996] suggests that partial melting may occur within the thermal boundary layer in regions where the overlying mantle is relatively hot [*Williams and Garnero*, 1996], and thus globally, the base of the mantle is probably near the solidus for at least some components of the mantle composition. This would tend to accentuate the viscosity reduction and lateral homogenization of the deeper parts of D" in all regions, even if they are cold enough to suppress extensive partial melting as appears to be the case in the relatively high velocity regions of all three of our study areas. Further work is needed to resolve the vertical distribution of heterogeneity within D".

Acknowledgments. We thank X.-F. Liu for providing his lower mantle shear velocity model prior to publication and Mike Kendall for providing D" thickness estimates in Figure 19. Many of the figures were made using the GMT mapping software of *Wessel and Smith* [1991]. Helpful comments were provided in the review process by Michael Wysession, Michael Weber, Tine Thomas, and an anonymous reviewer. This research was supported by NSF grants EAR 9305894 and EAR 9418643. Ed Garnero was supported by an NSF postdoctoral fellowship. Contribution 295 of the Institute of Tectonics and the W. M. Keck Seismological Laboratory.

References

Ding, X., and D. V. Helmberger, Modeling D" structure beneath Central America with broadband seismic data, *Phys. Earth Planet. Inter.*, in press, 1996.

Dziewonski, A. M., and D. L. Anderson, Preliminary reference Earth model, *Phys. Earth Planet. Inter.*, *25*, 297-356, 1981.

Gaherty, J. B., and T. Lay, Investigation of laterally heterogeneous shear velocity structure in D" beneath Eurasia, *J. Geophys. Res.*, *97*, 417-435, 1992.

Garnero, E. J., and D. V. Helmberger, Travel times of *S* and *SKS*: Implications for three-dimensional lower mantle structure beneath the central Pacific, *J. Geophys. Res.*, *98*, 8225-8241, 1993.

Garnero, E. J., and D. V. Helmberger, A very slow basal layer underlying large-scale low-velocity anomalies in the lower mantle beneath the Pacific: Evidence from core phases, *Phys. Earth Planet. Inter.*, *91*, 161-176, 1995.

Garnero, E. J., and D. V. Helmberger, Seismic detection of a thin laterally varying boundary layer at the base of the mantle beneath the central-Pacific, *Geophys. Res. Lett.*, *23*, 977-980, 1996.

Garnero, E. J, and T. Lay, Lateral variations in lowermost mantle shear wave anisotropy beneath the north Pacific and Alaska, *J. Geophys. Res.*, in press, 1997.

Garnero, E. J., D. V. Helmberger, and G. Engen, Lateral variations near the core-mantle boundary, *Geophys. Res. Lett.*, *15*, 609-612, 1988.

Garnero, E. J., D. V. Helmberger, and S. Grand, Preliminary evidence for a lower mantle shear wave velocity discontinuity beneath the central Pacific, *Phys. Earth Planet. Inter.*, *79*, 335-347, 1993.

Grand, S. P., Mantle shear structure beneath the Americas and surrounding oceans, *J. Geophys. Res.*, *99*, 11,591-11,622, 1994.

Helmberger, D. V., L.-S. Zhao, and E. Garnero, Construction of synthetics for 2D structures; core phases, in *Seismic Modeling of Earth Structure*, edited by E. Boschi, G. Ekström, and A. Morelli, pp. 183-222, Soc. Ital. di Fis., Rome, 1996.

Houard, S., and H.-C. Nataf, Further evidence for the 'Lay discontinuity' beneath Northern Siberia and the North Atlantic from short-period *P*-waves recorded in France, *Phys. Earth Planet. Inter.*, *72*, 264-275, 1992.

Houard, S., and H.-C. Nataf, Laterally varying reflector at the top of D" beneath northern Siberia, *Geophys. J. Int.*, *115*, 168-182, 1993.

Igel, H., and M. Weber, *P-SV* wave propagation in the Earth's mantle using finite differences: Application to heterogeneous lowermost mantle structure, *Geophys. Res. Lett.*, *23*, 415-418, 1996.

Kendall, J.-M., and C. Nangini, Lateral variations in D" below the Caribbean, *Geophys. Res. Lett.*, *23*, 399-402, 1996.

Kendall, J.-M., and P. M. Shearer, Lateral variations in D" thickness from long-period shear-wave data, *J. Geophys. Res.*, *99*, 11575-11590, 1994.

Kendall, J.-M., and P. M. Shearer, On the structure of the lowermost mantle beneath the southwest Pacific, southeast Asia and Australasia, *Phys. Earth Planet. Inter.*, *92*, 85-98, 1995.

Krüger, F., M. Weber, F. Scherbaum, and J. Schlittenhardt, Double beam analysis of anomalies in the core-mantle boundary region, *Geophys. Res. Lett.*, *20*, 1475-1478, 1993.

Krüger, F., M. Weber, F. Scherbaum, and J. Schlittenhardt, Evidence for normal and inhomogeneous lowermost mantle and core-mantle boundary structure under the Arctic and northern Canada, *Geophys. J. Int.*, *122*, 637-657, 1995.

Krüger, F., F. Scherbaum, M. Weber, and J. Schlittenhardt, Analysis of asymmetric multipathing with a generalization of the double-beam method, *Bull. Seismol. Soc. Am.*, *86*, 737-749, 1996.

Lavely, E. M., D. W. Forsyth, and P. Friedemann, Scales of heterogeneity near the core-mantle-boundary, *Geophys. Res. Lett.*, *13*, 1505-1508, 1986.

Lay, T., Localized velocity anomalies in the lower mantle, *Geophys. J. R. Astron. Soc.*, *72*, 483-516, 1983.

Lay, T., Evidence of a lower mantle shear velocity discontinuity in *S* and *sS* phases, *Geophys. Res. Lett.*, *13*, 1493-1496, 1986.

Lay, T., Structure of the core-mantle transition zone: A chemical and thermal boundary layer, *Eos Trans. AGU, 70(4)*, 49, 54-55, 58-59, 1989.

Lay, T., Seismology of the lower mantle and core-mantle boundary, *U.S. Natl. Rep. Int. Union Geod. Geophys. 1991-1994 Rev. Geophys.*, *33*, 325-328, 1995.

Lay, T., and D. V. Helmberger, A lower mantle *S*-wave triplication and the shear velocity structure of D", *Geophys. J. R. Astron. Soc.*, *75*, 799-838, 1983.

Lay, T., and C. J. Young, Analysis of seismic *SV* waves in the core's penumbra, *Geophys. Res. Lett.*, *18*, 1373-1376, 1991.

Lay, T., and C. J. Young, Imaging scattering structures in the lower mantle by migration of long-period *S* waves, *J. Geophys. Res.*, *101*, 20023-20040, 1996.

Li, X.-D., and B. Romanowicz, Global mantle shear velocity model developed using nonlinear asymptotic coupling theory, *J. Geophys. Res.*, *101*, 22245-22272, 1996.

Liu, X.-f., and A. M. Dziewonski, Lowermost mantle shear wave velocity structure, *Eos Trans. AGU, 75(44)*, Fall Meet. Suppl., 663, 1994.

Loper, D. E., and T. Lay, The core-mantle boundary region, *J. Geophys. Res.*, *100*, 6397-6420, 1995.

Masters, G., H. Bolton, and P. Shearer, Large-scale 3-dimensional structure of the mantle (abstract), *Eos Trans. AGU, 73(14)*, Spring Meet. Suppl., 201, 1992.

Nataf, H.-C., and S. Houard, Seismic discontinuity at the top of D": A world-wide feature?, *Geophys. Res. Lett.*, *20*, 2371-2374, 1993.

Revenaugh, J., and T. H. Jordan, Mantle layering from ScS reverberations, 4, The lower mantle and core-mantle boundary, *J. Geophys. Res.*, *96*, 19,811-19,824, 1991.

Schwartz, S. Y., T. Lay, and S. L. Beck, Shear wave travel time, amplitude, and waveform analysis for earthquakes in the Kurile slab: Constraints on deep slab structure and mantle heterogeneity, *J. Geophys. Res.*, *96*, 14,445-14,460, 1991a.

Schwartz, S. Y., T. Lay, and S. P. Grand, Seismic imaging of subducting slab structure: Trade-offs with deep path and near-receiver effects, *Geophys. Res. Lett.*, *18*, 1265-1268, 1991b.

Stacey, F. D., and D. E. Loper, The thermal boundary layer interpretation of D" and its role as a plume source, *Phys. Earth Planet. Inter.*, *33*, 45-55, 1983.

Su, W.-J., R. L. Woodward, and A. M. Dziewonski, Degree-12 model of shear velocity heterogeneity in the mantle, *J. Geophys. Res.*, *99*, 6945-6980, 1994.

Sylvander, M., and A. Souriau, Mapping *S* velocity heterogeneities in the D" region, from *SmKS* differential travel times, *Phys. Earth Planet. Inter.*, *94*, 1-21, 1996.

Thomas, C., and M. Weber, *P* velocity heterogeneities in the lower mantle determined with the German Regional Seismic Network: Improvement of previous models and results of 2D modeling, *Phys. Earth Planet. Inter.*, in press, 1996.

Vidale, J. E., and H. M. Benz, Seismological mapping of fine structure near the base of the Earth's mantle, *Nature*, *361*, 529-532, 1993.

Weber, M., *P* and *S* wave reflections from anomalies in the lowermost mantle, *Geophys. J. Int.*, *115*, 183-210, 1993.

Weber, M., and J. P. Davis, Evidence of laterally inhomogeneous lower mantle structure from *P* and *S* waves, *Geophys. J. Int., 102*, 231-255, 1990.

Weber, M., and M. Körnig, A search for anomalies in the lowermost mantle using seismic bulletins, *Phys. Earth Planet. Inter., 73*, 1-28, 1992.

Wessel, P., and W. H. F. Smith, Free software helps map and display data, *Eos Trans. AGU, 72*, 441, 445-446, 1991.

Williams, Q., and E. J. Garnero, On the possible origin of a seismically thin boundary layer at the base of the mantle, *Science, 273*, 1528-1530, 1996.

Woodward, R. L., and G. Masters, Lower-mantle structure from *ScS-S* differential travel times, *Nature, 352*, 231-233, 1991.

Wright, C., K. J. Muirhead, and A. E. Dixon, The *P* wave velocity structure near the base of the mantle, *J. Geophys. Res., 90*, 623-634, 1985.

Wysession, M. E., L. Bartko, and J. B. Wilson, Mapping the lowermost mantle using core-reflected shear waves, *J. Geophys. Res., 99*, 13667-13684, 1994.

Wysession, M. E., L. Bartko, and J. B. Wilson, Correction to "Mapping the lowermost mantle using core-reflected shear waves," *J. Geophys. Res., 100*, 8351, 1995a.

Wysession, M. E., R. W. Valenzuela, A.-N. Zhu, and L. Bartko, Investigating the base of the mantle using differential travel times, *Phys. Earth Planet. Inter., 92*, 67-84, 1995b.

Yamada, A., and I. Nakanishi, Detection of *P*-wave reflector in D" beneath the south-western Pacific using double-array stacking, *Geophys. Res. Lett., 23*, 1553-1556, 1996.

Young, C. J., and T. Lay, The core-mantle boundary, *Annu. Rev. Earth Planet. Sci., 15*, 25-46, 1987a.

Young, C. J., and T. Lay, Evidence for a shear velocity discontinuity in the lowermost mantle beneath India and the Indian Ocean, *Phys. Earth Planet. Inter., 49*, 37-53, 1987b.

Young, C. J., and T. Lay, Multiple phase analysis of the shear velocity structure in the D" region beneath Alaska, *J. Geophys. Res., 95*, 17,385-17,402, 1990.

J. B. Gaherty, Department of Earth, Atmospheric and Planetary Sciences, Massachusetts Institute of Technology, Rm 54-512, Cambridge, MA 02139. (e-mail: gaherty@quake.mit.edu)

E. J. Garnero and T. Lay, Institute of Tectonics, University of California, Earth and Marine Sciences Building, Santa Cruz, CA 95064. (e-mail: eddie@earthsci.ucsc.edu; thorne@earthsci.ucsc.edu)

C. J. Young, Geophysics Department 6116, Sandia National Laboratory, MS 0750, Albuquerque, NM 87185-5800. (e-mail: cjyoung@somnet.sandia.gov)

(Received July 18, 1996; revised December 27, 1996;
accepted January 31, 1997.)